SWS Beam Profiles and ISO Pointing

Status Report at the start of ISO Post-Operations Phase

Prepared by: Alberto Salama (ESA/SIDT/IDC)

September 9, 1998

1 Purpose

The purpose of this report is to present a summary of all observations performed to fully characterise the SWS Focal Plane Geometry, the SWS beam profiles and to improve the ISO pointing accuracy, together with the status of the data reduction and a plan for future work. Effort has been invested to distill as much as possible all the relevant information gathered during the ISO mission, with pointers to relevant references for the details. The final data analysis, culminating in the production of calibration files and software tools to improve the flux calibration of a given observation and the determination of surface brightness, is a work package for the Post Operation Phase, which will stay at the IDC (VILSPA) with the author, who has been responsible for all phases of this calibration programme, from the definition of the requirements (Ref. 1: IOCRD 6.4.1.1, 6.4.1.2, 6.4.2.1, 6.4.3.1), their implementation (see Ref. 2, IOCD respective sections), the preparation of the measurements themselves and their analysis.

2 Observations

2.1 Ground based testing

Prior to the ISO launch, no detailed calibration was available of the SWS beam profiles due to lack of a suitable point source in the ground based laboratory testing (ILTs).

2.2 Focal Plane Geometry

For an overview of the optical configuration of the SWS we refer to Table 1, taken from the SWS IDUM. The Focal Plane Geometry calibration has been performed within the ISO Satellite Commissioning Phase (REVs 12,14,17,18,19,20). See Ref. 2,3 for details and Table 2 for the Observations summary.

The offsets between each of the three SWS apertures and the ISO OSS Optical axis have been calibrated by making rasters maps around point-like sources, with the two SWS grating scanners set at fixed positions, corresponding to selected key wavelengths as defined in the flux calibration programme. In order to ensure the most accurate pointing, five guide stars were used. A special procedure was in place to insure quick turnaround times for the derivation and immediate application of the offsets.

The measurements were performed as follows: by means of square rasters around HR6705, one of the main SWS photometric calibrators, apertures 2,3 and 1 were calibrated in REV. 17. The offsets to the initial pointing were derived by the SIDT on the same day and used by the Spacecraft Control Centre (SCC) already the day after. These were verified with a finer square raster on aperture 2 and by cross-like rasters on the other two apertures.

In order to avoid possible effects specific to HR6705 and its associated guide stars for that day, other six point-like sources were used for further verification in REV. 19 and 20. All these measurements had been constructed via the Calibration Uplink System (CUS), as SWS AOTs do not allow measurements at fixed scanner positions and in raster mode.

The verification and fine tuning rasters were cross-like in order to optimise the use of time. The cross-like axis were parallel to the Y and Z axis of the spacecraft respectively. Each part of the cross consisted in a pair of scans, back and forward, in order to counteract possible detector hysterises effects. There exists two raster modes on ISO, one parallel to the spacecraft Y-axis (the longest side of the slit, along the SWS cross-dispertion direction) and one with a given orientation w.r.t. the Astronomical North (or=0 in Table 2). This second option was chosen, in order to ensure for both sides of the cross the back and forward configuration.

At the end of revolution 20, AOT 2 wavelength scans were perfomed at each side of the slits. As of revolution 21, the nominal pointing mode with one guide star was used, and the FPG was verified on HR6705 by means of a smaller square raster around it.

The FPG data analysis has been done by the SIDT following previoulsy written Calibration Analysis procedures (CAPs), stored in the SWS Interactive Analyisis (SIA). From the ERDs, produced by the OLP team on time scales much shorter than in normal operations ("fast-ERDs"), SPDs were derived within SIA. On the other side, the FPGC files, produced by SCC, contained the Y and Z coordinates and the time keys of each raster point. These were used to chop the SPD in pieces, each associated with the SWS detector signals corresponding to each raster point. The signals were averaged over each of the six SWS detector bands and contour plots were produced for the square rasters, and polynomial fits were made of the cross-like rasters. The 50% signal levels were used to determine the centroid points. For more details over the results, see Ref. 3,4,5,6.

The FPG calibration proved to be good the the arcsecond level already in REV 19 an no further updates were requested. The analysis of the REV20 raster however (done with one guide star) showed a -2 arcsec offset in the Z direction on HR6705, but this was judged by the SIDT not to be worth a further update to the FPG offsets.

2.3 FPG PV checks: cross-like rasters

As a further cross-check of the Focal Plane Geometry, dedicated cross-rasters were designed during the PV phase and inserted into the schedule. These were checks and therefore had to be short in time, however effort was invested to use these to prepare for the full characteristion of the beam profiles, planned to be over a number of wavelengths, covering also the FP range. Targets HR5340 and NML-CYG were used primarily for the grating and FP sections respectively.

At each raster point, the grating scanners were set to more than one fixed grating position, thus covering more than one pair of wavelengths, in general chosen to be the same key wavelengths as defined in the flux calibration programme. Being short checks, however, no back-forward scans were performed, and therefore the two sides of the cross were commanded to be parallel to the Y-axis.

2.4 Beam Profiles Large Scale calibration

The beam profiles were fully characterised as layed down in the IOCD sections 6.4.1.1 and 6.4.1.2, with fixed grating scanner positions, corresponding to the flux calibration key wavelengths and with rectangular rasters covering at least one diffraction beam outside the slit. Only small adjustements to the raster parameters were necessary, following the results of the preparatory crosses. Target HR5340 was used for the grating section and NML-CYG and ETA CAR for the FP section.

2.5 Beam Profiles Small Scale calibration: AOT1 and CUS AOT1-like sparse maps

The beam profiles depend on wavelength, clearly from AOT band to AOT band when either detector band or slit size change (cf. Table 1), but also in general within an AOT band, due to the dependency of the diffraction profile on wavelength. For this purpose were the AOT1 maps performed.

The first exercise of this kind was performed early in REV126, around HR6705. This consisted in a series of 7 quick (=speed 1) AOT1's performed as a cross-like shape covering the size of the smallest SWS aperture.

However, a pointing offset became apparent as well as an offset between detector bands which did not allow to cover both sides of the profile (see Fig. 20).

A second and finer map was done on HR5340 later in REV244, but the results showed some inconsistency. Later on it was found that HR5340, being bright in the visible, was causing read-out blooming effects on the Star Tracker CCD, if used at time of the year when the orientation of the STR was parallel to the line of sight defined by HR5340 and the guide star used (Ref. 8)

This type of exercise was then suspended, waiting for possible improvement of the ISO pointing accuracy. Once achieved, three further exercises were perfomed to characterise the small scale beam profile close to the peak, via 5X5 rasters done at 2 arseconds steps on HR5340 (REV 640) and NML-CYG (REV 742) for the grating and FP sections respectively. A third exercise was done later on in REV 860, on HR1457 (for visibility reasons) to characterise on a fine scale the full wavelength dependency in the Z direction covering both sides of the profile. For time economy reasons, all these wavelength scans were made coarser than the fastest AOT1. Via the CUS, an AOT1-like was constructed by setting the grating scanner step size to 6 (instead of 4 for a speed 1 AOT1) and repeated in a raster pattern.

2.6 SSO Tracking corrections: subarcsec scale Z-axis beam profile

ISO tracked Solar System Objects by means of successive linear rasters. The raster parameters were computed by the mission planning software so that on each raster leg the SSO was allowed to drift from -1 to +1 arcseconds (prior to its improvement in revolution via SCREW 254, the tracking was between 0 and 2 arcseconds). Dedicated measurements were performed in revolution 769 to characterise the beam profile on the subarsecond level. See Ref. 19 for details.

2.7 Straylight from out of field sources characterisation

Out of beam radiation levels were characterised early in PV phase as layed down in IOCD section 6.4.3.1 on the bright source W HYA, down to 2 arcminutes distance from it. Later in the mission, specific straylight checks were performed, prompted by science needs for better characterise the influence of straylight for planet satellites such as Titan and Europa.

In REV. 384 the bright spectral line at 13.7 μm of the C_2H_2 molecule was observed on Saturn and at a position relative to Saturn, corresponding to Titan's western elongation of 3 arcminutes (Y_off = -87 arcsec, Z_off = - 163 arcsec), but with Titan far off the aperture, a few days later than the science observation on Titan. This gave a rejection factor of 10^4. Other two intermediate positions were chosen, coinciding with positions relative to Saturn as used in the beam profile full characterisation.

The search for water lines at 39.37 and 43.89 μm prompted for a pair of on-off measurements at Titan's Eastern elongation in June 1997 (revs. 579 and 581). These checks, lasting no more than 20 minutes each, were performed within the SWS Calibration time budget and consisted in 4 AOT2 up-down scans across the 39.37 μm line and 3 up-down scans across the 43.89 μm line. More extensive measurements of the background at the position of Titan's western elongation at those wavelengths were performed within the solicited time programme ZZH2O and are described in Ref. 7.

2.8 Introduction of the Virtual Aperture 4

The characterisation of the SWS beam profiles in the PV phase revealed a significant offset of detector band 6 with respect to the others (-9 arcseconds in Y direction), implying a signal loss of about 30Via SCREW 187 virtual aperture 4 was introduced for the FP observations to correct for this offset. This was verified in Rev. 161 with a sequence of AOT7's pointed at each side of the target NML-CYG along the Y axis and by a rectangular raster performed with the CUS, with grating and FP kept at fixed positions. Table 2 lists the observational details.

2.9 ISO Pointing improvement

The beam profiles measurements, the AOT1 maps, the Instrumental Line Profile pointing induced effects characterisations on IC2501, some flux and wavelength calibration observations, all pointed to the suspect that errors of up to 4 arcseconds could be present in the ISO pointing, dependent on the target observed. Pointing appeared to be better than the specification (Absolute Pointing Error (APE) of 11.7 arcseconds), but it was suspected by the SIDT that some systematics could be present, which could therefore be corrected for.

A specific calibration programme was designed and executed in REV 137, by which a number of point-like sources were observed with ISOCAM. A simple configuration was chosen in order to fit as many as possible stars in a time deemed reasonable for such an erercise. Four hours were allocated by the Project Scientist for this experiment, as additional ISO calibration time. 79 stars, selected by the CIDT from the GBPP programme, were observed in the LW9 filter (at 15 μm). The centroids of all these images were derived by the CIDT. 54 stars gave good centroid determination. These were correlated by the author with (i) the position of the guide star in the STR field of view, (ii) star ecliptical and galactic coordinates, (iii) the Solar Aspect Angle, and (iv) guide star magnitudes. The experiment and its analysis are described in Ref. 17. It appeared that some correlation was present with the position of the guide star in the STR field of view, but the S/N ratio was not very convincing, but still indicative of a possible improvement in the ISO pointing. A second attempt was made later in Rev. 264, with a more accurate star selection procedure taken by the author, based on the Hipparcos star catalogue and an ad-hoc empirical colour-colour relation between visual magnitude (quoted in the HIC) and the expected flux in CAM LW9 filter. This second experiment is described in ref. 18 and was also confined to last 4 hours. This time a convincing relation was found between pointing offset and the position of the guide star in the STR field of view.

SCC initiated then an independent programme based on the absolute pointing reconstruction as given by the confirmation star, a second guide star used at the start of every revolution. This is described in Ref. 13. It appeared that a recalibration of the STR was possible, via the introduction of a focal length dependence on the angle of incidence of the visible radiation coming from the guide star. The model was applied to predict the offsets as measured in the REV264 experiment done with ISOCAM and the agreement with the measured offsets was excellent (see ref. 11).

SCREW 280 was raised to introduce the improvement in the ISO uplink. A verification exercise was designed by the SIDT and described down below in par. 4.2. The STR recalibration became operative as of REV369. A second, but of lower magnitude, improvement in the ISO pointing has been obtained by increasing the sampling of the Sun ephemerides as used by the on board software of the AOCS – ISO Z-axis has to point always towards the Sun. As of Revolution 451, a new so-called Sun-model was introduced, by which AOCS on-board Sun ephemerides related parameters were updated 4 times each revolution (ref. 10). The improved pointing algorithm (ref. 14) was also introduced in the downlink in OLP V6.1.

2.10 Pointing effects on fringes

The effect of pointing offsets on the position and intensity of the instrumental fringes, most prominent in AOT band 3A, was characterised with dedicated spectral scans performed at various positions with respect to NML-CYG. The experiments and the associated data analysis results are given in Ref. 15 and 16.

2.11 Pointing effects on the Instrumental Line Profile

The effects of pointing offsets on the Instrumental Line Profile has been characterised with a dedicated series of pointing around the bright line-emission and point-like object IC2501 early in PV phase. See Ref. 5 for details on the experiment and its result.

3 Data reduction

A consistent reprocessing of all beam profile related observations has started. In this report, results are presented of all CUS rasters and AOT1 observations, for which SPDs and IIPH files were available as produced with pipeline version greater or equal than 6.1, i.e. with the pointing reconstruction algorithm. This means all such measurements, excluding the FPG ones. These will be re-reduced once reprocessed with OLP V7.0.

Effort has been put in documenting the data reduction steps in dedicated CAPs. Two classes of CAPs were written, one for the CUS rasters (with fixed grating position) and one for the AOT1 and CUS AOT1-like maps. These can be found in appendix I. The reduced data have been stored as structures, in .xdr IDL save sets, for future processing.

These are of the form:

- CUS rasters with fixed grating scanner position(s).

  For each TDT and grating scanner position,

```
|-HEADER<Strng>(1)
|---WAVE<Float>(6)
|---DATA<Struc>(m*n)
                           |-Y_OFFSET<Float>(1)
                           |-Z_OFFSET<Float>(1)
                           |------DET<Struc>(52)
                                                    |--FLUX<Float>(1)
                                                    |-STDEV<Float>(1)
```

where HEADER is the SPD header and WAVE stores the wavelengths associated with each of the six detector bands corresponding to the grating scanner position, as relevant. The DATA part is a substructure, storing for each raster point the median Y and Z offsets as derived from the IIPH, and for each detector element, the median signal and standard deviation (in μV/s), after neglecting the first 5 seconds, the time needed for AOCS stabilisation after moving to that raster point (see also figs. 22 to 25).

- AOT1 and CUS AOT1-like maps For each TDT (i.e. aperture),

```
(m*n)
     |-Y_OFFSET<Float>(1)
     |-Z_OFFSET<Float>(1)
     |----BANDS<Struc>(12)
                         |------NAME<Strng>(1)
                         |----FACTOR<Float>(1)
                         |-INTERCEPT<Float>(1)
                         |-----SLOPE<Float>(1)
```

giving for each point of the map the Y_OFFSET and Z_OFFSET, as the medians of the values derived from the respective IIPH file, and for each AOT band the result of a first order polynomial fit across the AOT band (flux vs. wavelength): the average flux across the AOT band, normalised to the on-target position (FACTOR), the INTERCEPT of the fit at the lower AOT band wavelength border, and the fit SLOPE.

4 Discussion

4.1 Beam Profiles calibration

The result of the consistent processing of the data sets are shown in figures 1 to 21. Data sets taken on different sources at different times show very good agreements in the beam profile shapes. This is valid within the apertures sizes, as shown in the plots on a linear scale, as well as beyond, as shown in the plots on a logarithmic scale for which the profile is measured over 3 orders of magnitudes. The profiles are seen to be quite narrow toward the peak, with a somewhat triangular shape along the Y-axis, expecially remarkable for Band 1, for which a 4 arcsecond offset w.r.t. the peak results in about 20% signal loss. For the other bands, the Z-direction (the shortest side of the slit) is the most sensitive to small pointing offsets, giving rise to inaccuracies of the absolute flux level of the order of 30% at the longests wavelengths.

The pointing reconstruction algorithm applied to early mission data sets give pointing offsets ranging from around -3 to 3 arcseconds in both Y and Z direction, and it is remarkable that when corrected for those offsets, all profile centres tend to concentrate towards consistent values. Detector band to band offsets clearly appear from all these measurements. As a given target cannot therefore be centred exactly for all detector bands, signal losses due to the narrow beam profiles arise. For some bands, small pointing offsets can have an amplified effect on the absolute photometric level. The exact determination of these signal losses and band to band offsets has been attempted in the course of the mission, however no proper fitting/interpolation routine has been found, which can successfully been used on the peaked beam profiles to allow for an accurate determination of the centroid and therefore of the true peak signal. Attempts were made to derive a model of the beam profiles, by convolution of the theoretical telescope diffraction profile with the nominal SWS aperture profile. The version currently in SIA (Ref. 2) has been proven however not yet appropriate to describe the narrow, triangular shaped profile. The consistency shown by the reprocessing exercise described here is however promisising and a strategy for deriving accurate beam profiles, band to band offsets and associated signal losses is outlined below. As a first approximation, a visual inspection of the plots give the following:

```
Detector band offsets and signal losses: first order assessment

                   ----------------------------------------------
                   Band      Y_offset        Z_offset   Signal
                             (arcsec)        (arcsec)   Loss
                   ----------------------------------------------
                     1        0               0           0 %
                     2       -1               0          <10 %
                     3       -1.5 +/- 0.5    -2           10...20%
                     4       +3.5 +/- 1.5    -3 +/- 1     20...30%
                   ----------------------------------------------
```

4.2 ISO Pointing Improvement

The verification of the STR recalibration done in rev 368/369 via SWS AOT2s around HR6705 (see par. 2.9) resulted in a go-ahead for its implementation in the ISO Uplink. The data reduction done at that time is described in Ref. 9. With the old STR calibration, the measured offsets from HR6705 were of 3.3 and -3.3 arcseconds along the Y and Z axis respectively. With the new calibration, these amounted to 2.4 and -1.0 arcseconds respectively. Some of the residuals were attributed to inaccuracies in the Sun model, first improved in REV451. This can account for some of this, but a residual of the level of about 1.5 arcseconds remains. This is the quoted accuracy of the ISO pointing after the improvements (ref. 12). A trend analysis study of a number of routine flux calibration monitoring with HR6705 shows however that this residual could be specific to HR6705 and the specific guide star used at that time, due to aberration effects not taken into account yet. See Ref. 20 for more details on this.

The agreement of the various SWS beam profile centroids as seen in the plots shown in this report taken on various celestial targets, when corrected for the offsets derived from the pointing improvement reconstruction algorithm, the reduced scatter in the SWS photometric calibration monitoring observations (see Refs. 20 and 24) after introduction of the pointing recalibration in the Uplink, the explanation of the pointing errors as seen with the Rev. 264 CAM experiment by the pointing recalibration algorithm derived via the confirmation stars, are all independent confirmations that this was a true improvement in the ISO pointing. As pointed out in Ref. 20 however, there is scope for further improvements, if guide star quality, aberration, proper motion and parallax are taken into account.

4.3 Beam Profile Wavelength Dependency

The AOT1 exercises can be used for the characterisation of the beam profile wavelength dependence within an AOT band. This is done by fitting a first order polynomial the flux (in Jy) as a function of wavelength.

Only Band 2C clearly show a clear dependance of the fit parameters on the offset from the target (HR5340 – Fig. 17, or NML-CYG). It is to be confirmed whether this is not caused by detector hysterises effects (unlikely, as only the down scan only has been used in the reduction and also because the pattern is symmetric around the target) or more likely by the fact that the large wavelength range covered by this AOT band. The average signals across each AOT bands are shown in figure 18 for the HR5340 experiment and Fig. 19 for the NML-CYG experiment. The HR6705 experiment is shown in Fig. 20. The sections along the Z-axis around the targets are overplotted onto the HR1457 experiment in fig. 21. In here the HR6705 set has been shifted by the amount given by the pointing reconstruction algorithm, 1.3 arseconds. The agreement between these different data sets is almost perfect. It is apparent that this could be even better if account is taken of the current quoted pointing accuracy of ISO, 1.5 arcseconds. In fact, best agreement for the data sets on HR5340 and NML CYG can be reached by shifting each other by 1 arcsecond along the Y axis and -2 arcseconds along the Z axis.

4.4 SWS AAR Pointing Offset Correction Tool

The availability of small scale characterisation of the beam profiles led to the development of an SIA tool which could correct for the wavelength dependent beam profile AARs with given pointing offsets, calculated in Y,Z coordinate space from product header entries. The tool is currently under development (see Ref. 23)

4.5 Pointing jitter induced correlated noise correction

The ISO Pointing jitter is seen by the SWS detectors as the target moves across the beam profile, and result in a detector band correlated noise. This is illustrated in the case of CUS rasters done at fixed grating scanner position, shown in figure 22 to 25. For each detector band, the 12 detector elements signals show very similar time behaviour over the time in which the SWS is kept fixed at each raster position, i.e. about 20 seconds. The average jitter across the signal median is clearly following the IIPH time behaviour. This noise is of the order of a few percent of the median flux (peak to peak). This correlated noise is further discussed in Ref. 21 in the case of SWS AOTs.

5 Conclusions: foreseen future work

A consistent characterisation of the SWS Beam profiles has been demonstrated to be possible from the measurements presented in this report. I envisage two calibration files to store the wavelength dependent SWS beam profiles, one around the peak, finely sampled (0.1 arseconds) and one extending far off the wings of the beam, coarsly sampled (4 arcseconds). These should be of the same structure (as defined for the AOT1 experiments) but should be separated because of computing speed efficiency and because of different useage: The small scale beams will be used to correct absolute flux levels due to mispointing of any given observation, via the AAR pointing correction tool. The signal changes due to the SSO tracking may also be corrected via this file, e.g. by allowing the pointing correction tool to accept Y,Z offsets as time dependent, as derived from the IIPH file. Another application of this file is the improvement of the S/N ratio of a given observation, via elimination of the detector band correlated noise due to pointing jitter via a second tool. Finally, the large scale beam profile calibration file may be used to derive surface brightness values for extended sources, via deconvolution, obtained via a third tool.

In order to arrive to the final calibration files, ideally one should take each reduced data set, now easily available as structures stored in IDL .xdr save sets, and relate it to the beam profile model (once improved within IA). The data set should be shifted around by amounts comparable with the current ISO pointing accuracy, until finding best agreement with the model. Once determining the true peak, the profile would be normalised. This operation would be repeated for all data sets.

The current SWS beam profile model cannot however successfully explain the triangular shape of the cross-dispertion profiles, particularly evident at the short wavelengths. In fact, this can be an input to the model.

Therefore, the approach which will be taken to obtain the beam profiles calibration files will be to combine all the measurements taken, via interpolation. This is corroborated by the general self-consistency shown in this report. The various data sets will be first shifted/renormalised to take account of the ISO pointing accuracy. The extrapolation to the far wings of the profiles will be done via the model.

In parallel, effort should be in place to further improve the pointing accuracy of ISO, by taking into account guide star quality, aberration, proper motion and parallax. The latter three are addressed by SCREW 359.

6 References

1. "ISO In Orbit Calibration Requirements Document (IOCRD)", ISO-SSD-9003

2. "ISO-SWS In Orbit Calibration Document (IOCD)", ISO-94-23, Version 1.0, 7-JUN-1995

3. "ISO Launch and Early Orbit Phase & Satellite Commissioning Phase Report", D/TOS-ISO-LEOP/SCP/JF, Issue 1, 31-OCT-1997.

4. "SWS PV Performance Report", status at REV 56, 12-JAN-1996

5. "SWS PV Report", 9-OCT-1996

6. "SWS SCP and PV Revolution Folders"

7. A. Coustenis, A. Salama, E. Lellouch, et al., "Evidence for water vapor in Titan's atmosphere from ISO/SWS data" A&A, 336, L85-L89 (1998)

8. Schmidt, M. "Mappings in revolution 452/ impact of bright sources on the [STR] CCD", MS/960218-1, 18-FEB-97.

9. Salama, A. "The Rev. 368/369 ISO STR calibration adjustement verification experiment", 28-NOV-1996

10. Schuetz, A. "Accuracy of sun motion model", FCSD/VILSPA/as-29, 23-OCT-1996

11. Schmidt, M. "Correlation between 'AOCS pointing accuracy experiment' and 'CAM pointing experiment', MS/961029-1, 29-OCT-1996

12. Faelker, J., Viewgraphs presented at the ISO Celebration hold on 2-3 April 1998, VILSPA

13. Casale, M., "Investigations about the ISO pointing accuracy", mc-18-10, 19-OCT-96

14. Stephenson, C.A., "Viewing Direction Correction Algorithm", 29-APR-97

15. Haser, L., "Relation between fringe structure and pointing in AOT-band 3A", 6-AUG-1997

16. Haser, L., "Note on the pointing raster for NML-CYG, parallel to the dispersion", 5-DEC-1997

17. Salama, A., "Report on the REV137 ISO pointing accuracy experiment", 26-APR-1996

18. Salama, A., "Report on the REV264 ISO pointing accuracy experiment", 24-OCT-1996

19. Vandenbussche, B., "The SWS Z-beam-profile for SSO tracking correction", SWS EOM

20. Feuchtgruber, H., "Status of study on Gam-Dra fluxes and related pointing errors", SWS EOM

21. Heras, A. M., "The effects of the pointing jitter on SWS observations", SWS EOM

22. Beintema, D.,A., "sws_beam" SIA routine

23. Cami, J, "The AAR pointing correction tool", SWS EOM (TBW)

24. Morris, P. "SWS Flux calibration", SWS EOM

Table 1: Detector definition for the SWS AOT bands

	AOT band	order	aperture		filter	area[5] ($'' \times ''$)	detector type	detector number	wavelength (μm)
SW	1A	4	1	t	Al_2O_3	14-20	InSb	1 - 12	2.38 - 2.60
SW	1B	3	1	t	Al_2O_3	14-20	InSb	1 - 12	2.60 - 3.02
SW	1D	3	2	t	LiF	14-20	InSb	1 - 12	3.02 - 3.52
SW	1E	2	2	t	LiF	14-20	InSb	1 - 12	3.52 - 4.08
SW	2A	2	2	t	LiF	14-20	Si:Ga	13 - 24	4.08 - 5.30
SW	2B	1	2	t	LiF	14-20	Si:Ga	13 - 24	5.30 - 7.00
SW	2C	1	3	t	SrF_2	14-20	Si:Ga	13 - 24	7.00 - 12.0
LW	3A	2	1	r	Al_2O_3	14-27	Si:As	25 - 36	12.0 - 16.5
LW	3C	2	2	r	LiF	14-27	Si:As	25 - 36	16.5 - 19.5
LW	3D	1	2	r	LiF	14-27	Si:As	25 - 36	19.5 - 27.5
LW	3E	1	3	r	SrF_2	20-27	Si:As	25 - 36	27.5 - 29.0
LW	4	1	3	r	SrF_2	20-33	Ge:Be	37 - 48	29.0 - 45.2
F-P1	5A	3	1	r	Al_2O_3	10-39	Si:Sb	49 - 50	11.4 - 12.2
F-P1	5B	2	1	r	Al_2O_3	10-39	Si:Sb	49 - 50	12.2 - 16.0
F-P1	5C	2	2	r	LiF	10-39	Si:Sb	49 - 50	16.0 - 19.0
F-P1	5D	1	2	r	LiF	10-39	Si:Sb	49 - 50	19.0 - 26.0
F-P2	6	1	3	r	SrF_2	17-40	Ge:Be	51 - 52	26.0 - 44.5

Notes:

1. SW = short-wavelength grating region

2. LW = long-wavelength grating region

3. t = transmission

4. r = reflection

5. 'Aperture area' refers to the nominal dimensions of the SWS detector bands projected on the sky.

6. Detector 49 is used for FP observations in band 5.

7. Detector 51 is used for FP observations in band 6.

Table 2. Observations Summary

Focal Plane Geometry Calibration (5 guide stars)

REV	TDT	OSN	RA hh mm ss.ss	AOT	DEC d ' ''	I time h m s	UTC start	target	m	n	dm	dn	rol	or
012	001	01	17 55 38.99	S99	+51 32 36.8	2 08 53	29 Nov 1995 08 34 45	GAM-DRA	11	11	6	6	0	1
014	008	01	19 34 19.70	S99	+51 14 12.0	2 09 02	01 Dec 1995 10 56 14	GAMMA-DRA	11	11	9	9	0	1
017	001	01	17 55 46.95	S99	+51 31 42.6	2 08 52	04 Dec 1995 08 16 11	GAM-DRA	11	11	6	6	0	1
017	003	01	17 55 46.95	S99	+51 31 42.6	2 08 52	04 Dec 1995 11 40 51	GAM-DRA	11	11	9	9	0	1
017	007	01	17 55 48.16	S99	+51 31 33.1	2 08 52	04 Dec 1995 20 12 33	GAM-DRA	11	11	6	6	0	1
018	001	01	17 55 36.33	S99	+51 31 49.8	2 08 52	05 Dec 1995 08 13 34	GAM-DRA	11	11	4	4	0	1
018	004	01	19 36 13.49	S99	+50 18 19.1	0 30 18	05 Dec 1995 11 46 12	R-CYG	12	2	4	2	129	0
018	005	02	19 36 13.49	S99	+50 18 19.1	0 29 14	05 Dec 1995 12 17 16	R-CYG	12	2	3	2	39	0
018	006	03	19 36 13.49	S99	+50 18 19.1	0 30 18	05 Dec 1995 12 53 44	R-CYG	12	2	4	2	129	0
018	007	04	19 36 13.49	S99	+50 18 19.1	0 29 14	05 Dec 1995 13 24 48	R-CYG	12	2	3	2	39	0
018	008	05	19 36 49.39	S99	+50 11 59.5	0 30 18	05 Dec 1995 13 59 18	R-CYG	12	2	4	2	129	0
018	009	06	19 36 49.39	S99	+50 11 59.5	0 30 48	05 Dec 1995 14 30 22	R-CYG	12	2	3	2	39	0
018	012	01	19 37 22.30	S99	+50 18 29.9	0 30 18	05 Dec 1995 17 56 12	GAMMA-DRA	12	2	4	2	107	0
018	013	02	17 56 36.40	S99	+51 29 20.3	0 29 14	05 Dec 1995 18 27 16	GAMMA-DRA	12	2	3	2	17	0
018	014	03	17 56 36.40	S99	+51 29 20.3	0 30 18	05 Dec 1995 19 03 16	GAMMA-DRA	12	2	4	2	107	0
018	015	04	17 56 36.40	S99	+51 29 20.3	0 29 14	05 Dec 1995 19 34 20	GAMMA-DRA	12	2	3	2	17	0
018	016	05	17 56 36.40	S99	+51 29 20.2	0 30 18	05 Dec 1995 20 10 20	GAMMA-DRA	12	2	4	2	107	0
018	017	06	17 56 36.40	S99	+51 29 20.3	0 30 48	05 Dec 1995 20 41 24	GAMMA-DRA	12	2	3	2	17	0
019	001	01	17 29 30.44	S99	+52 21 03.9	0 30 18	06 Dec 1995 08 10 29	BET-DRA	12	2	4	2	100	0
019	002	02	17 30 25.99	S99	+52 18 05.0	0 29 14	06 Dec 1995 08 41 33	BET-DRA	12	2	3	2	10	0
019	003	03	17 30 25.99	S99	+52 18 05.0	0 30 18	06 Dec 1995 09 17 33	BET-DRA	12	2	4	2	100	0
019	004	04	17 30 25.99	S99	+52 18 05.0	0 29 14	06 Dec 1995 09 48 37	BET-DRA	12	2	3	2	10	0
019	005	05	17 30 25.99	S99	+52 18 05.0	0 30 18	06 Dec 1995 10 24 37	BET-DRA	12	2	4	2	100	0
019	006	06	17 30 25.99	S99	+52 18 05.0	0 30 48	06 Dec 1995 10 55 41	BET-DRA	12	2	3	2	10	0
019	011	01	17 30 25.99	S99	+52 18 05.0	0 30 18	06 Dec 1995 14 04 27	KSI-DRA	12	2	4	2	105	0
019	012	02	17 53 31.66	S99	+56 52 21.2	0 29 14	06 Dec 1995 14 35 31	KSI-DRA	12	2	3	2	15	0
019	013	03	17 53 31.67	S99	+56 52 21.2	0 30 18	06 Dec 1995 15 16 01	KSI-DRA	12	2	4	2	105	0
019	014	04	17 53 31.66	S99	+56 52 21.2	0 30 48	06 Dec 1995 15 47 05	KSI-DRA	12	2	3	2	15	0
019	019	01	19 12 33.07	S99	+67 39 41.2	0 30 18	06 Dec 1995 18 53 41	DEL-DRA	12	2	4	2	123	0
019	020	02	19 12 33.08	S99	+67 39 41.1	0 29 14	06 Dec 1995 19 24 45	DEL-DRA	12	2	3	2	33	0
019	021	03	19 12 33.07	S99	+67 39 41.2	0 30 18	06 Dec 1995 20 00 45	DEL-DRA	12	2	4	2	123	0
019	022	04	19 12 33.08	S99	+67 39 41.1	0 30 48	06 Dec 1995 20 31 49	DEL-DRA	12	2	3	2	33	0
020	001	01	12 19 11.24	S99	+48 52 19.4	0 30 18	07 Dec 1995 08 07 54	3-CVN	12	2	4	2	30	0
020	002	02	12 19 48.70	S99	+48 59 02.8	0 29 14	07 Dec 1995 08 38 58	3-CVN	12	2	3	2	120	0
020	003	03	12 19 48.70	S99	+48 59 02.8	0 30 18	07 Dec 1995 09 14 58	3-CVN	12	2	4	2	30	0
020	004	04	12 19 48.70	S99	+48 59 02.8	0 29 14	07 Dec 1995 09 46 04	3-CVN	12	2	3	2	120	0
020	005	05	12 19 48.70	S99	+48 59 02.8	0 30 18	07 Dec 1995 10 21 04	3-CVN	12	2	4	2	30	0
020	006	06	12 19 48.70	S99	+48 59 02.8	0 30 48	07 Dec 1995 10 52 08	3-CVN	12	2	3	2	120	0
020	011	01	12 19 48.70	S99	+48 59 02.8	0 30 18	07 Dec 1995 14 02 18	CF-BOO	12	2	4	2	52	0
020	012	02	14 08 17.32	S99	+49 27 29.0	0 29 14	07 Dec 1995 14 33 22	CF-BOO	12	2	3	2	142	0
020	013	03	14 08 17.32	S99	+49 27 29.0	0 30 18	07 Dec 1995 15 13 40	CF-BOO	12	2	4	2	52	0
020	014	04	14 08 17.32	S99	+49 27 29.0	0 30 48	07 Dec 1995 15 44 44	CF-BOO	12	2	3	2	142	0
020	019	01	14 08 17.32	S02	+49 27 29.1	0 09 36	07 Dec 1995 18 25 54	CF-BOO						
020	020	02	14 08 17.32	S02	+49 27 36.1	0 09 36	07 Dec 1995 18 36 14	CF-BOO-7N						
020	021	03	14 08 16.62	S02	+49 27 29.1	0 09 36	07 Dec 1995 18 46 32	CF-BOO-7E						
020	022	04	14 08 17.32	S02	+49 27 22.1	0 09 36	07 Dec 1995 18 56 52	CF-BOO-7S						
020	023	05	14 08 18.02	S02	+49 27 29.1	0 09 36	07 Dec 1995 19 07 10	CF-BOO-7W						
020	034	01	15 24 55.80	S02	+58 57 57.7	0 09 36	07 Dec 1995 20 11 30	IOT-DRA						
020	035	02	15 24 55.80	S02	+58 57 57.7	0 09 36	07 Dec 1995 20 21 50	IOT-DRA-7N						
020	036	03	15 24 55.80	S02	+58 58 04.7	0 09 36	07 Dec 1995 20 32 08	IOT-DRA-7E						
020	037	04	15 24 55.80	S02	+58 58 04.7	0 09 36	07 Dec 1995 20 42 28	IOT-DRA-7S						
020	038	05	15 24 56.70	S02	+58 57 57.7	0 09 36	07 Dec 1995 20 52 46	IOT-DRA-7W						

Focal Plane Geometry Verification (One Guide Star)

REV	TDT	OSN	RA	AOT	DEC	I time	UTC start	target	m	n	dm	dn	rol	or
			hh mm ss.ss		d ' ''	h m s								
021	005	01	17 56 36.40	S99	+51 29 20.3	0 16 22	08 Dec 1995 08 20 39	GAMMA-DRA	5	5	4	4	0	1
021	006	02	17 56 36.40	S99	+51 29 20.3	0 15 10	08 Dec 1995 08 37 47	GAMMA-DRA	5	5	4	4	0	1
021	007	03	17 56 36.40	S99	+51 29 20.3	0 16 32	08 Dec 1995 08 53 41	GAMMA-DRA	5	5	4	4	0	1

FPG checks via cross-like rasters

REV	TDT	OSN	RA	AOT	DEC	I time	UTC start	target	m	n	dm	dn	rol	or
			hh mm ss.ss		d ' ''	h m s								
024	013	01	17 56 36.40	S99	+51 29 20.3	0 21 16	11 Dec 1995 19 16 58	HR6705	5	1	5	2	0	1
024	014	02	17 56 36.40	S99	+51 29 20.3	0 21 32	11 Dec 1995 19 38 58	HR6705	1	5	2	3	90	1
028	002	01	15 50 46.59	S99	+48 28 58.7	0 21 16	15 Dec 1995 07 22 52	ST-HER	5	1	5	2	74	1
028	003	02	15 50 46.59	S99	+48 28 58.7	0 21 32	15 Dec 1995 07 44 50	ST-HER	1	5	2	3	164	1
032	014	01	15 50 46.59	S99	+48 28 58.7	0 25 06	19 Dec 1995 20 57 39	ST-HER	5	1	5	2	74	1
032	015	02	15 50 46.59	S99	+48 28 58.7	0 25 20	19 Dec 1995 21 23 27	ST-HER	1	5	2	3	164	1
036	008	01	14 15 40.01	S99	+19 11 04.7	0 26 28	23 Dec 1995 11 11 17	HR5340	7	1	4	2	0	1
036	009	02	14 15 40.01	S99	+19 11 04.7	0 26 52	23 Dec 1995 11 38 31	HR5340	1	7	2	6	0	1
036	023	01	20 46 25.50	S99	+40 06 59.4	0 26 30	23 Dec 1995 19 19 37	NML-CYG	7	1	4	2	0	1
036	024	02	20 46 25.50	S99	+40 06 59.4	0 26 54	23 Dec 1995 19 46 51	NML-CYG	1	7	2	6	0	1
040	030	01	20 46 25.50	S99	+40 06 59.4	0 06 46	27 Dec 1995 21 52 29	NML-CYG	7	1	4	2	0	1
040	031	02	20 46 25.50	S99	+40 06 59.4	0 06 58	27 Dec 1995 21 59 59	NML-CYG	1	7	2	6	0	1
044	008	01	10 45 03.60	S99	-59 41 04.3	0 31 20	31 Dec 1995 08 53 03	ETA-CAR	11	1	8	2	0	1
044	009	02	10 45 03.60	S99	-59 41 04.3	0 22 34	31 Dec 1995 09 25 11	ETA-CAR	1	7	2	4	0	1
044	022	01	20 46 25.50	S99	+40 06 59.4	0 14 26	31 Dec 1995 18 34 45	NML-CYG	5	1	5	2	131	0
044	023	02	20 46 25.50	S99	+40 06 59.4	0 14 38	31 Dec 1995 18 49 55	NML-CYG	5	1	2	3	41	0

Beam profile full calibrations

REV	TDT	OSN	RA	AOT	DEC	I time	UTC start	target	m	n	dm	dn	rol	or
			hh mm ss.ss		d ' ''	h m s								
048	011	01	20 46 25.50	S99	+40 06 59.4	0 46 54	04 Jan 1996 17 42 29	NML-CYG	14	11	6	4	0	1
048	012	01	20 46 25.50	S99	+40 06 59.4	0 56 16	04 Jan 1996 18 30 13	NML-CYG	14	9	6	4	0	1
048	013	01	20 46 25.50	S99	+40 06 59.4	0 25 02	04 Jan 1996 19 27 19	NML-CYG	9	8	8	6	0	1
056	002	01	10 45 03.60	S99	-59 41 04.3	0 25 04	12 Jan 1996 06 05 13	ETA-CAR	9	8	8	6	0	1
060	004	01	14 15 40.01	S99	+19 11 04.6	1 02 32	16 Jan 1996 09 59 35	HR5340	13	11	4	4	0	1
060	005	01	14 15 40.01	S99	+19 11 04.6	2 00 44	16 Jan 1996 11 02 57	HR5340	13	11	4	4	0	1
060	007	01	14 15 40.01	S99	+19 11 04.6	1 54 30	16 Jan 1996 13 51 57	HR5340	15	9	4	4	0	1

AOT1 and CUS AOT1-like beam profile calibrations

REV	TDT	OSN	RA	AOT	DEC	I time	UTC start	target	m	n	dm	dn	rol	or
			hh mm ss.ss		d ' ''	h m s								
126	011	17	17 56 37.01	S01	+51 29 20.3	0 17 42	22 Mar 1996 05 32 19	HR6705 6-0						
126	012	16	17 56 36.71	S01	+51 29 20.3	0 17 42	22 Mar 1996 05 50 45	HR6705 3-0						
126	013	15	17 56 36.41	S01	+51 29 20.3	0 17 42	22 Mar 1996 06 09 09	HR6705 0-0						
126	014	18	17 56 36.11	S01	+51 29 20.3	0 17 42	22 Mar 1996 06 27 35	HR6705 -3-0						
126	015	19	17 56 35.81	S01	+51 29 20.3	0 17 42	22 Mar 1996 06 45 59	HR6705 -6-0						
126	016	20	17 56 36.41	S01	+51 29 23.3	0 17 42	22 Mar 1996 07 04 25	HR6705 0-3						
126	017	21	17 56 36.41	S01	+51 29 17.3	0 17 42	22 Mar 1996 07 22 49	HR6705 0--3						
244	024	62	14 15 40.47	S01	+19 11 00.6	0 19 00	17 Jul 1996 23 25 08	HR5340_+0_-8						
244	025	63	14 15 40.37	S01	+19 11 01.4	0 19 00	17 Jul 1996 23 44 52	HR5340_+0_-6						
244	026	64	14 15 40.27	S01	+19 11 02.1	0 19 00	18 Jul 1996 00 04 34	HR5340_+0_-4						
244	027	65	14 15 40.07	S01	+19 11 02.9	0 19 00	18 Jul 1996 00 24 18	HR5340_+0_-2						
244	028	66	14 15 39.97	S01	+19 11 03.6	0 19 00	18 Jul 1996 00 44 00	HR5340 ALF-BOO						
244	029	67	14 15 39.87	S01	+19 11 04.4	0 19 00	18 Jul 1996 01 03 44	HR5340_+0_+2						
244	030	68	14 15 39.66	S01	+19 11 05.1	0 19 00	18 Jul 1996 01 23 26	HR5340_+0_+4						
244	031	69	14 15 39.57	S01	+19 11 05.8	0 19 00	18 Jul 1996 01 43 10	HR5340_+0_+6						
244	032	70	14 15 39.47	S01	+19 11 06.6	0 19 00	18 Jul 1996 02 02 52	HR5340_+0_+8						
244	033	71	14 15 40.17	S01	+19 11 11.0	0 19 00	18 Jul 1996 02 22 36	HR5340_+8_+0						
244	034	72	14 15 39.77	S01	+19 10 56.2	0 19 00	18 Jul 1996 02 42 18	HR5340_-8_+0						
640	001	01	14 15 39.88	S99	+19 11 01.4	1 59 22	16 Aug 1997 20 33 12	HR5340	5	5	2	2	0	1
640	002	02	14 15 39.88	S99	+19 11 01.4	2 46 52	16 Aug 1997 22 33 16	HR5340	5	5	2	2	0	1
640	003	03	14 15 39.88	S99	+19 11 01.4	2 46 02	17 Aug 1997 01 20 52	HR5340	5	5	2	2	0	1
641	001	01	14 15 39.58	S01	+19 11 07.0	0 19 00	17 Aug 1997 20 29 53	HR5340 (+0, +7)						
641	001	02	14 15 40.58	S01	+19 11 05.6	0 19 00	17 Aug 1997 20 49 35	HR5340 (+0, -7)						
641	001	03	14 15 40.18	S01	+19 11 16.2	0 19 00	17 Aug 1997 21 09 19	HR5340 (+10, 0)						
641	001	04	14 15 39.98	S01	+19 10 56.4	0 19 00	17 Aug 1997 21 29 01	HR5340 (-10, 0)						
742	001	01	19 42 04.10	S99	+55 27 47.0	2 11 52	26 Nov 1997 14 01 24	NML-CYG	5	5	2	2	0	1
742	002	02	19 42 04.10	S99	+55 27 47.0	2 11 52	26 Nov 1997 16 13 58	NML-CYG	5	5	2	2	0	1
742	003	03	19 42 04.10	S99	+55 27 47.0	2 13 32	26 Nov 1997 18 26 34	NML-CYG	5	5	2	2	0	1
860	024	01	04 35 55.19	S99	+16 30 33.7	1 27 16	24 Mar 1998 18 33 21	HR1457	2	9	2	2	0	1
860	025	02	04 35 55.19	S99	+16 30 33.7	2 01 27	24 Mar 1998 20 01 21	HR1457	2	9	2	2	0	1
860	026	03	04 35 55.19	S99	+16 30 33.7	1 58 36	24 Mar 1998 22 03 32	HR1457	2	9	2	2	0	1

Subarcsecond scale Z-axis beam profile for SSO Tracking Correction

REV	TDT	OSN	RA	AOT	DEC	I time	UTC start	target
			hh mm ss.ss		d ' ''	h m s		
769	002	01	01 18 33.70	S99	-00 09 42.4	0 13 06	23 Dec 1997 12 41 37	VESTA
769	003	01	01 18 33.90	S99	-00 09 38.7	0 12 20	23 Dec 1997 12 55 29	VESTA
769	004	01	01 18 34.20	S99	-00 09 34.9	0 12 20	23 Dec 1997 13 08 49	VESTA
769	005	01	01 18 34.50	S99	-00 09 31.1	0 12 20	23 Dec 1997 13 22 09	VESTA
769	006	01	01 18 34.70	S99	-00 09 27.4	0 12 20	23 Dec 1997 13 35 29	VESTA
769	007	01	01 18 35.00	S99	-00 09 23.6	0 12 20	23 Dec 1997 13 48 49	VESTA
769	008	01	01 18 35.20	S99	-00 09 19.9	0 12 21	23 Dec 1997 14 02 09	VESTA
769	009	01	01 18 35.50	S99	-00 09 16.1	0 12 20	23 Dec 1997 14 15 30	VESTA
769	010	01	01 18 35.70	S99	-00 09 12.4	0 12 20	23 Dec 1997 14 28 50	VESTA
769	011	01	01 18 35.90	S99	-00 09 08.6	0 12 20	23 Dec 1997 14 42 10	VESTA
769	012	01	01 18 36.20	S99	-00 09 04.6	0 13 04	23 Dec 1997 14 55 30	VESTA

Straylight checks

REV	TDT	OSN	RA	AOT	DEC	I time	UTC start	target	m	n	dm	dn	rol	or
			hh mm ss.ss		d ' ''	h m s								
056	008	01	13 49 02.09	S99	-28 22 03.0	0 24 56	12 Jan 1996 09 07 37	W-HYA	5	1	60	2	0	1
056	009	02	13 49 02.09	S99	-28 22 03.0	0 25 18	12 Jan 1996 09 33 25	W-HYA	1	5	2	60	90	1
384	017	67	00 06 28.90	S02	-01 58 16.1	0 04 04	04 Dec 1996 15 09 27	SATURN/TITAN OFF						
384	018	68	00 06 31.60	S02	-02 00 16.3	0 04 04	04 Dec 1996 15 14 21	SATURN/TITAN OFF						
384	019	69	00 06 23.40	S02	-02 00 42.5	0 04 04	04 Dec 1996 15 19 15	SATURN/TITAN OFF						
384	020	70	00 06 21.40	S02	-02 00 23.4	0 04 02	04 Dec 1996 15 24 07	SATURN/TITAN OFF						
384	021	71	00 06 19.40	S02	-02 00 04.2	0 04 04	04 Dec 1996 15 28 57	SATURN/TITAN OFF						
384	022	72	00 06 19.40	S02	-02 00 04.1	0 04 04	04 Dec 1996 15 33 43	SATURN						
524	004	02	21 24 30.80	S02	-15 49 44.9	0 48 49	23 Apr 1997 03 44 26	200502 EUROPA						
524	005	03	21 24 42.26	S02	-15 48 45.7	0 06 42	23 Apr 1997 04 34 07	200500 JUPITER						
524	043	04	21 24 28.30	S02	-15 49 55.5	0 48 50	23 Apr 1997 19 08 01	EUROPA-OFF						
579	002	02	01 12 42.40	S02	+05 08 30.6	0 29 16	17 Jun 1997 00 18 09	SATURN-OFF						
582	007	06	01 13 38.63	S02	+05 13 20.2	0 29 16	20 Jun 1997 13 18 51	200606 TITAN						

Verification of SCREW 187 implementation (Aperture 4)

REV	TDT	OSN	RA	AOT	DEC	I time	UTC start	target	m	n	dm	dn	rol	or
			hh mm ss.ss		d ' ''	h m s								
161	004	01	20 46 25.50	S99	+40 06 59.4	0 12 36	26 Apr 1996 01 35 54	NML-CYG	7	3	5	5	0	1
161	005	30	20 46 25.60	S07	+40 06 59.4	0 04 30	26 Apr 1996 01 49 12	NML-CYG-0						
161	006	31	20 46 25.60	S07	+40 06 54.4	0 04 30	26 Apr 1996 01 54 24	NML-CYG-+5						
161	007	32	20 46 25.70	S07	+40 06 49.4	0 04 30	26 Apr 1996 01 59 36	NML-CYG-+10						
161	008	33	20 46 25.60	S07	+40 07 04.4	0 04 30	26 Apr 1996 02 04 48	NML-CYG--5						
161	009	34	20 46 25.50	S07	+40 07 09.4	0 04 30	26 Apr 1996 02 10 00	NML-CYG--10						

Verification of the ISO pointing improvement (SCREW 280)

REV	TDT	OSN	RA	AOT	DEC	I time	UTC start	target
			hh mm ss.ss		d ' ''	h m s		
368	001	39	17 56 36.50	S02	+51 29 14.8	0 04 02	18 Nov 1996 11 48 26	HR6705_-4_4
368	002	40	17 56 36.20	S02	+51 29 17.0	0 04 02	18 Nov 1996 11 53 12	HR6705_0_4
368	003	41	17 56 35.80	S02	+51 29 19.2	0 04 02	18 Nov 1996 11 57 58	HR6705_4_4
368	004	42	17 56 36.00	S02	+51 29 22.5	0 04 02	18 Nov 1996 12 02 44	HR6705_4_0
368	005	43	17 56 36.30	S02	+51 29 25.8	0 04 02	18 Nov 1996 12 07 30	HR6705_4_-4
368	006	44	17 56 36.60	S02	+51 29 23.6	0 04 02	18 Nov 1996 12 12 16	HR6705_0_-4
368	007	45	17 56 37.00	S02	+51 29 21.4	0 04 02	18 Nov 1996 12 17 02	HR6705_-4_-4
368	008	46	17 56 36.80	S02	+51 29 18.1	0 04 02	18 Nov 1996 12 21 48	HR6705_-4_0
368	009	47	17 56 36.60	S02	+51 29 19.2	0 04 02	18 Nov 1996 12 26 34	HR6705_-2_0
368	010	48	17 56 36.30	S02	+51 29 18.6	0 04 02	18 Nov 1996 12 31 20	HR6705_0_2
368	011	49	17 56 36.20	S02	+51 29 21.4	0 04 02	18 Nov 1996 12 36 06	HR6705_2_0
368	012	50	17 56 36.50	S02	+51 29 22.0	0 04 02	18 Nov 1996 12 40 52	HR6705_0_-2
368	013	51	17 56 36.40	S02	+51 29 20.3	0 04 02	18 Nov 1996 12 45 38	HR6705
369	001	52	17 56 36.50	S02	+51 29 14.8	0 04 04	19 Nov 1996 11 45 29	HR6705_-4_4

```
369|002|53|17 56 36.20|S02  |+51 29 17.0|0 04 04|19 Nov 1996 11 50 15|HR6705_0_4
369|003|54|17 56 35.80|S02  |+51 29 19.2|0 04 04|19 Nov 1996 11 55 01|HR6705_4_4
369|004|55|17 56 36.00|S02  |+51 29 22.5|0 04 04|19 Nov 1996 11 59 47|HR6705_4_0
369|005|56|17 56 36.30|S02  |+51 29 25.8|0 04 04|19 Nov 1996 12 04 33|HR6705_4_-4
369|006|57|17 56 36.60|S02  |+51 29 23.6|0 04 04|19 Nov 1996 12 09 19|HR6705_0_-4
369|007|58|17 56 37.00|S02  |+51 29 21.4|0 04 04|19 Nov 1996 12 14 05|HR6705_-4_-4
369|008|59|17 56 36.80|S02  |+51 29 18.1|0 04 04|19 Nov 1996 12 18 51|HR6705_-4_0
369|009|60|17 56 36.60|S02  |+51 29 19.2|0 04 04|19 Nov 1996 12 23 37|HR6705_-2_0
369|010|61|17 56 36.30|S02  |+51 29 18.6|0 04 04|19 Nov 1996 12 28 23|HR6705_0_2
369|011|62|17 56 36.20|S02  |+51 29 21.4|0 04 04|19 Nov 1996 12 33 09|HR6705_2_0
369|012|63|17 56 36.50|S02  |+51 29 22.0|0 04 04|19 Nov 1996 12 37 55|HR6705_0_-2
369|013|64|17 56 36.40|S02  |+51 29 20.3|0 04 04|19 Nov 1996 12 42 41|HR6705
---|---|--|-----------|-----|-----------|-------|--------------------|-------------------------
```

Pointing effects on fringes

```
-------------------------------------------------------------------------------------------------
REV TDT OSN    RA      AOT      DEC      I time     UTC start         target      m  n dm dn rol or
           hh mm ss.ss        d  '  ''  h  m  s
---|---|--|-----------|-----|-----------|-------|--------------------|-----------------------------

587|031|01|20 46 25.50|S99  |+40 06 59.4|1 22 36|25 Jun 1997 09 59 54|NML-CYG     7  1  2  2   0  1
706|014|01|20 46 25.50|S99  |+40 06 59.4|0 58 24|21 Oct 1997 23 18 03|NML-CYG     1  5  2  2   0  1
---|---|--|-----------|-----|-----------|-------|--------------------|-----------------------------
```

Pointing effects on the Instrumental Line Profile

```
-------------------------------------------------------------------------------------------------
REV TDT OSN    RA      AOT      DEC      I time     UTC start         target
           hh mm ss.ss        d  '  ''  h  m  s
---|---|--|-----------|-----|-----------|-------|--------------------|-----------------------------
044|002|81|09 38 47.50|S02  |-60 05 28.1|0 21 00|31 Dec 1995 06 40 39|IC2501
044|003|82|09 38 47.50|S02  |-60 05 24.1|0 21 00|31 Dec 1995 07 02 23|IC2501-000
044|004|83|09 38 48.00|S02  |-60 05 26.9|0 21 00|31 Dec 1995 07 24 07|IC2501-072
044|005|84|09 38 47.80|S02  |-60 05 31.3|0 21 00|31 Dec 1995 07 45 51|IC2501-144
044|006|85|09 38 47.20|S02  |-60 05 31.3|0 21 00|31 Dec 1995 08 07 35|IC2501-216
044|007|86|09 38 47.00|S02  |-60 05 26.9|0 21 00|31 Dec 1995 08 29 19|IC2501-288
---|---|--|-----------|-----|-----------|-------|--------------------|-----------------------------
```

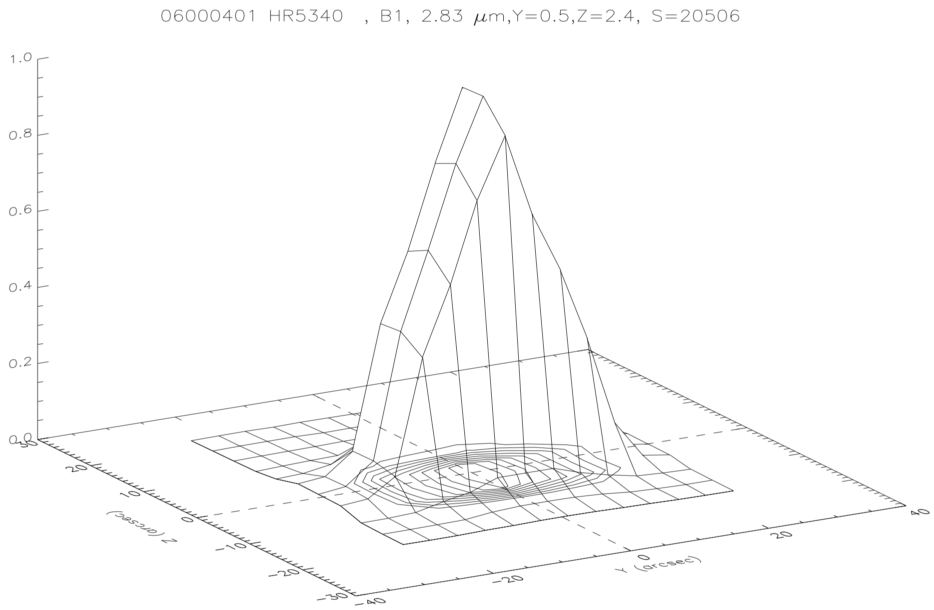

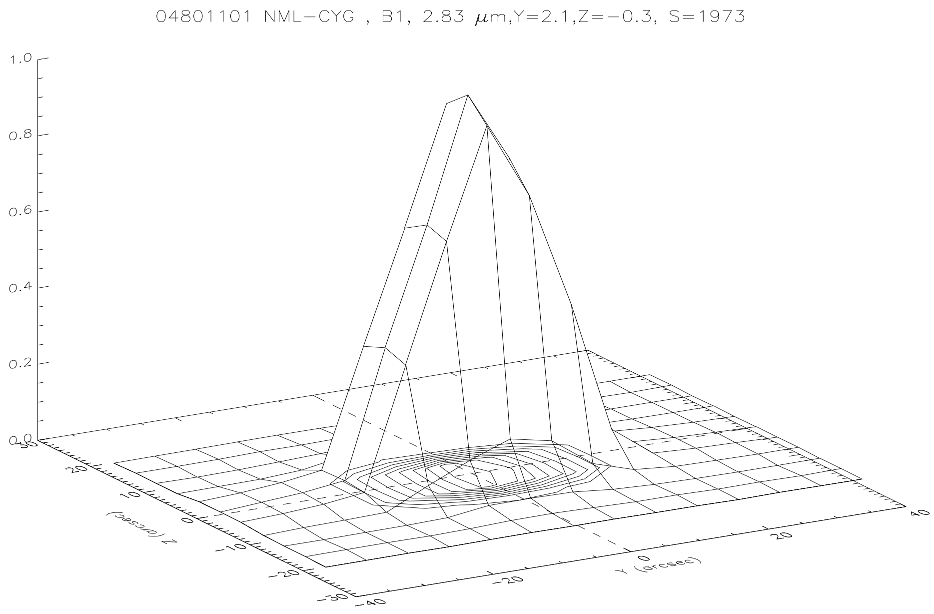

Figure 1: Beam profiles for Band 1, normalised to the maximum signal, given in the plot title (in μV/s). Contour plots are in steps of 10%, starting at 90% from the peak signal. The profiles have been shifted by the Y,Z offsets indicated, as provided by the pointing reconstruction algorithm (OLP Version $\geq$ 6.1)

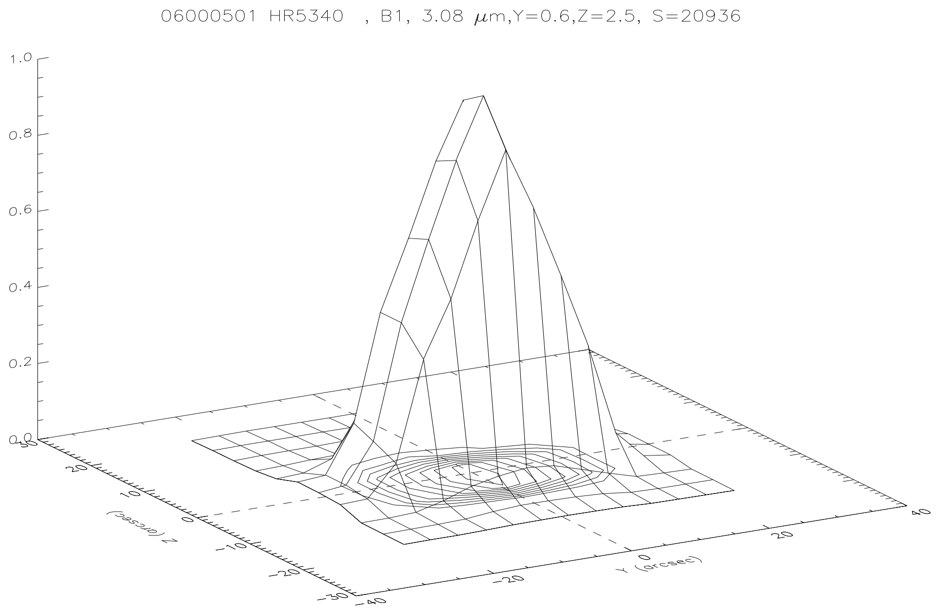

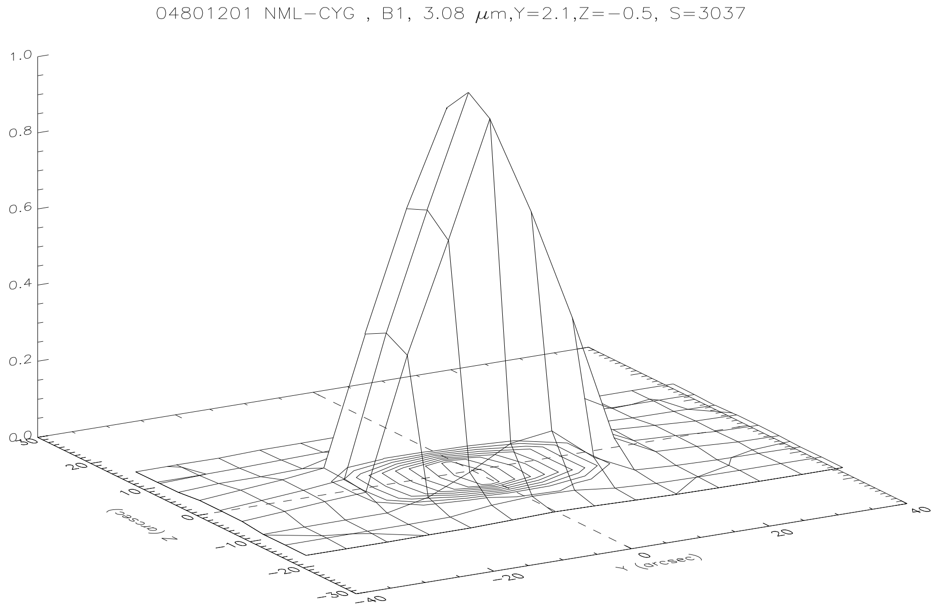

Figure 2: Beam profiles for Band 1, normalised to the maximum signal, given in the plot title (in μV/s). Contour plots are in steps of 10%, starting at 90% from the peak signal. The profiles have been shifted by the Y,Z offsets indicated, as provided by the pointing reconstruction algorithm (OLP Version $\geq$ 6.1)

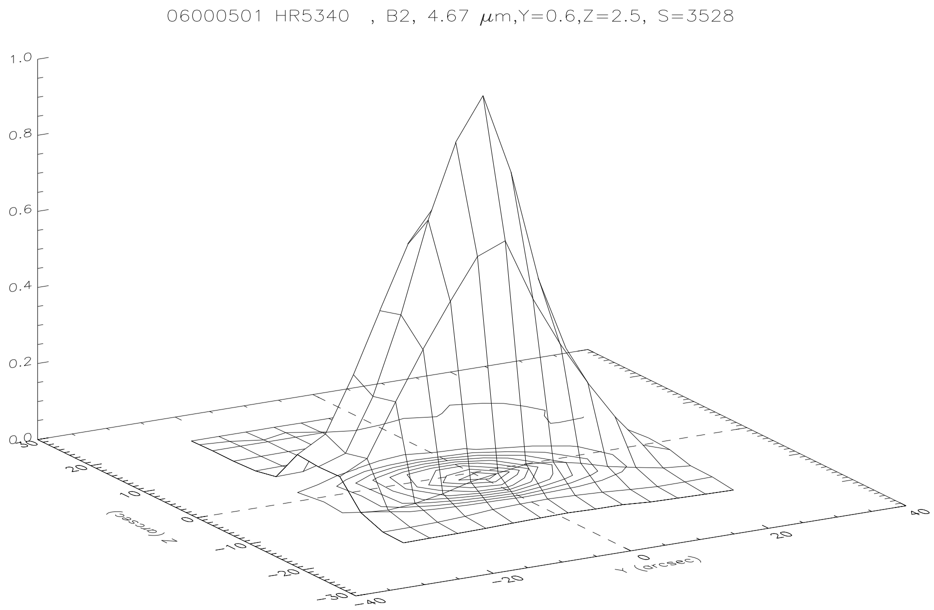

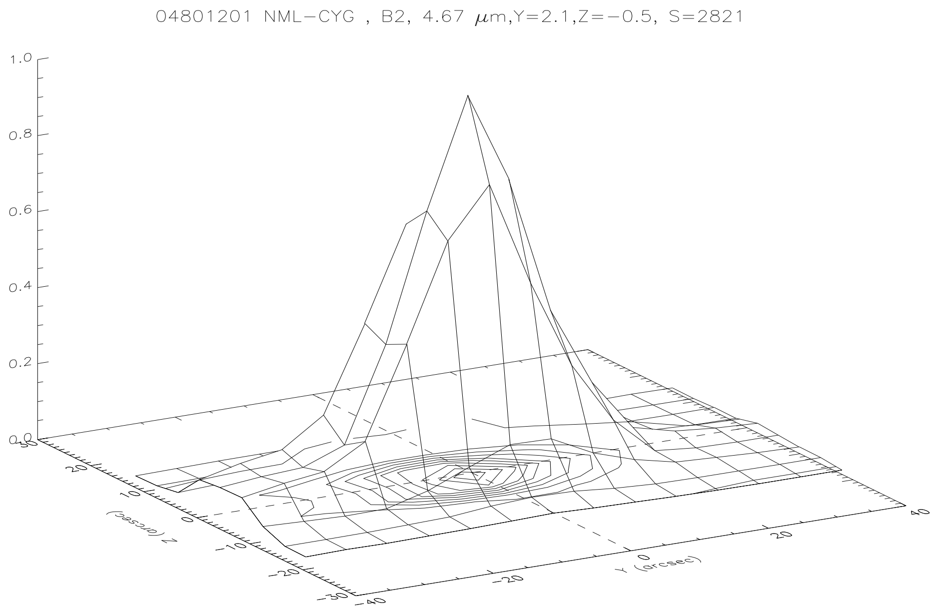

Figure 3: Beam profiles for Band 2, normalised to the maximum signal, given in the plot title (in μV/s). Contour plots are in steps of 10%, starting at 90% from the peak signal. The profiles have been shifted by the Y,Z offsets indicated, as provided by the pointing reconstruction algorithm (OLP Version $\geq$ 6.1)

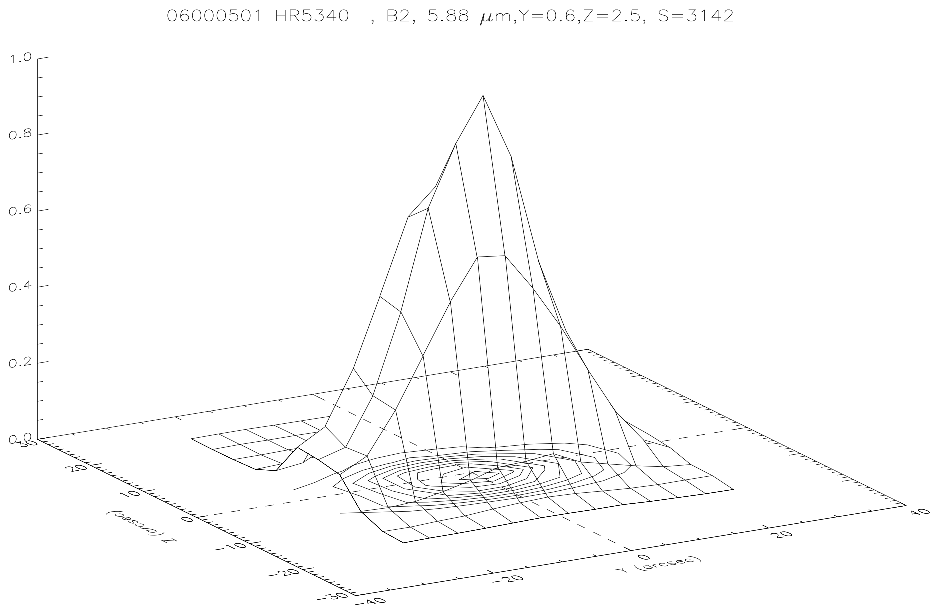

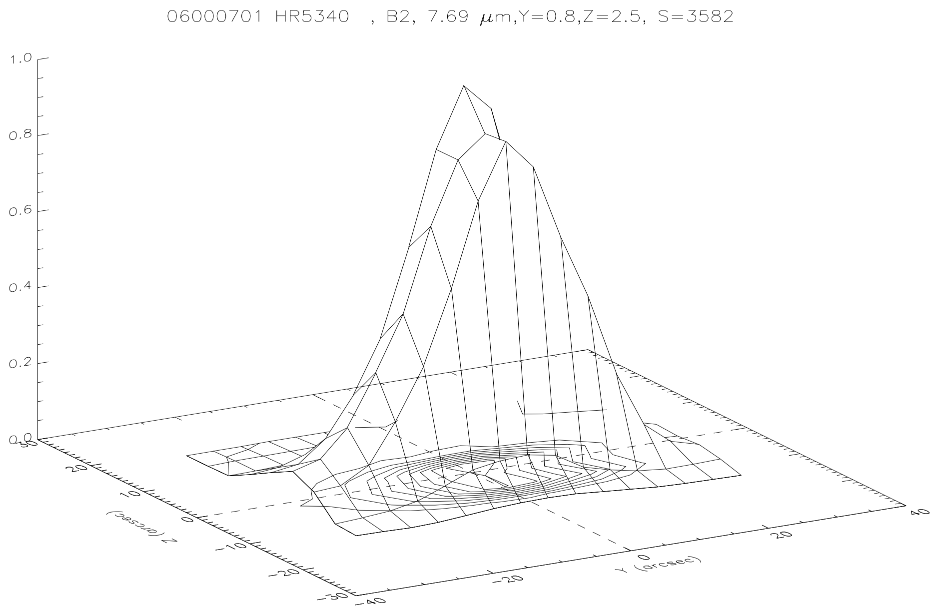

Figure 4: Beam profiles for Band 2, normalised to the maximum signal, given in the plot title (in μV/s). Contour plots are in steps of 10%, starting at 90% from the peak signal. The profiles have been shifted by the Y,Z offsets indicated, as provided by the pointing reconstruction algorithm (OLP Version $\geq$ 6.1)

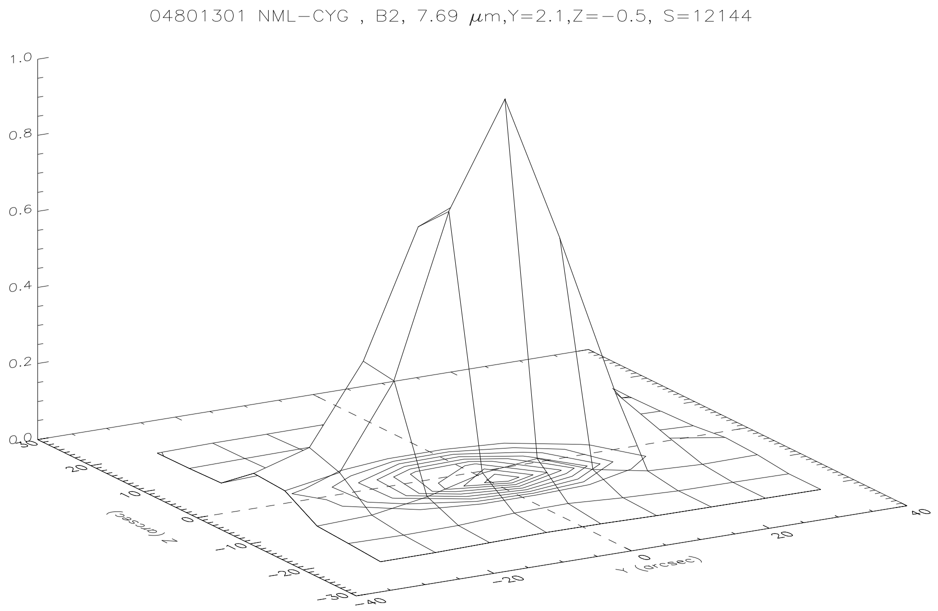

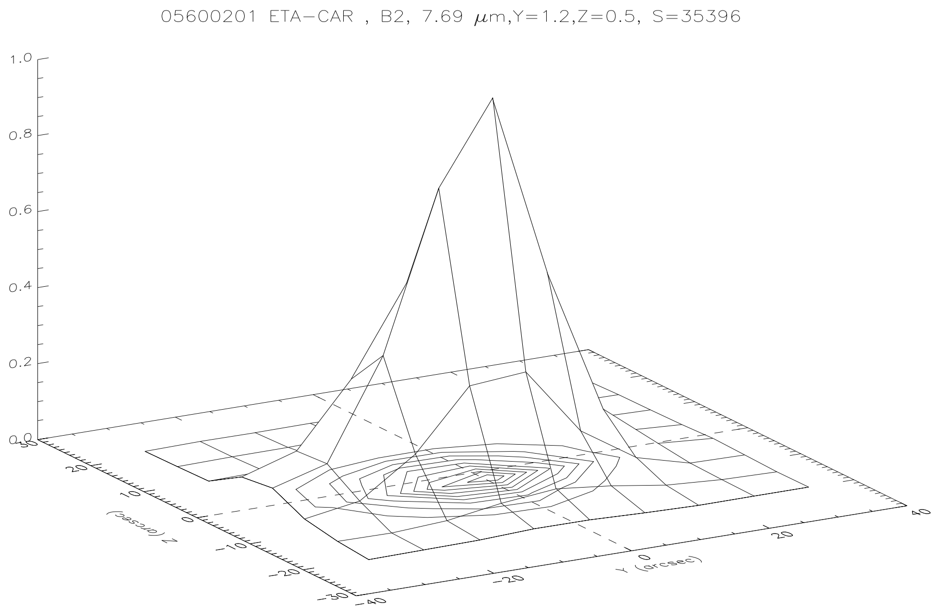

Figure 5: Beam profiles for Band 2, normalised to the maximum signal, given in the plot title (in μV/s). Contour plots are in steps of 10%, starting at 90% from the peak signal. The profiles have been shifted by the Y,Z offsets indicated, as provided by the pointing reconstruction algorithm (OLP Version $\geq$ 6.1)

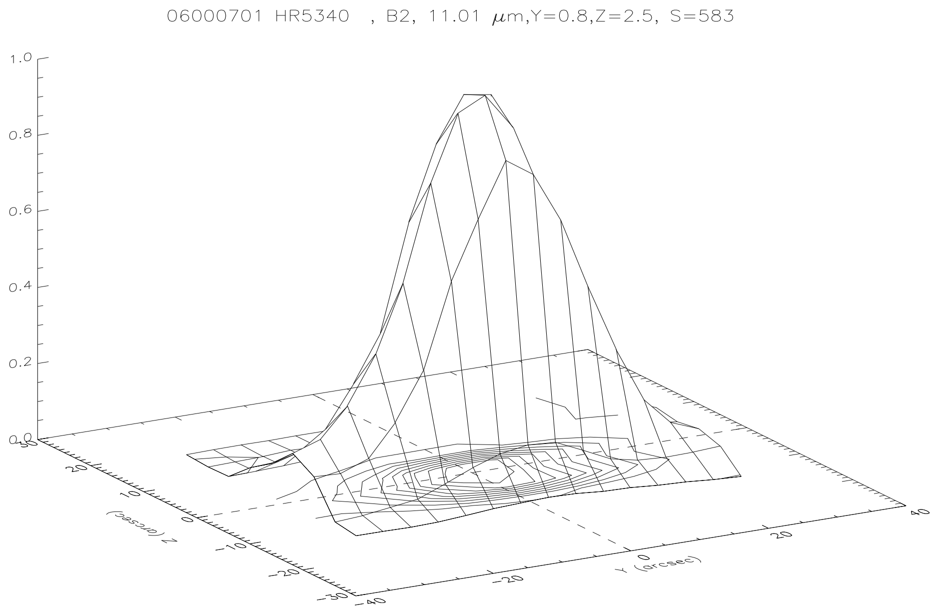

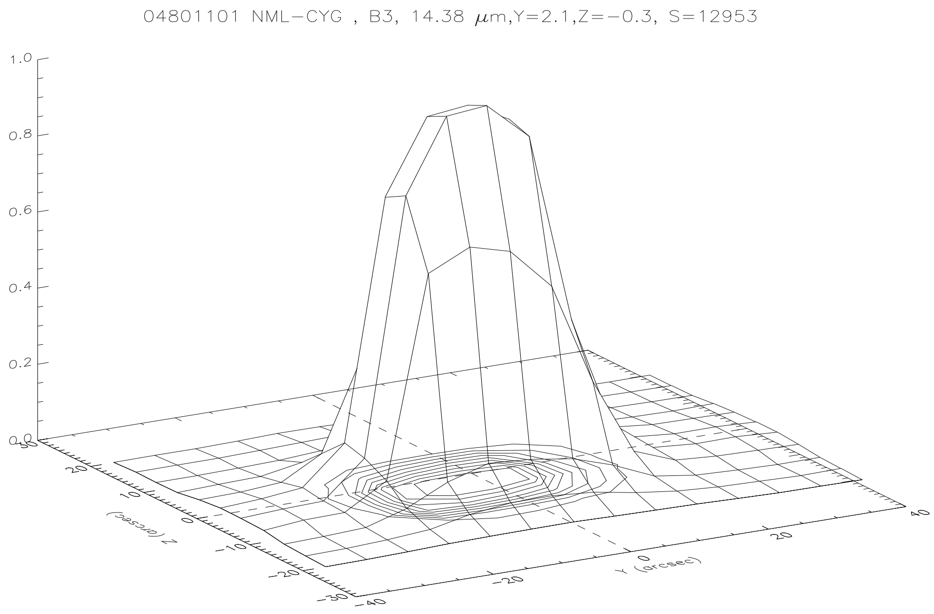

Figure 6: Beam profiles for Bands 2 and 3, normalised to the maximum signal, given in the plot title (in μV/s). Contour plots are in steps of 10%, starting at 90% from the peak signal. The profiles have been shifted by the Y,Z offsets indicated, as provided by the pointing reconstruction algorithm (OLP Version $\geq$ 6.1)

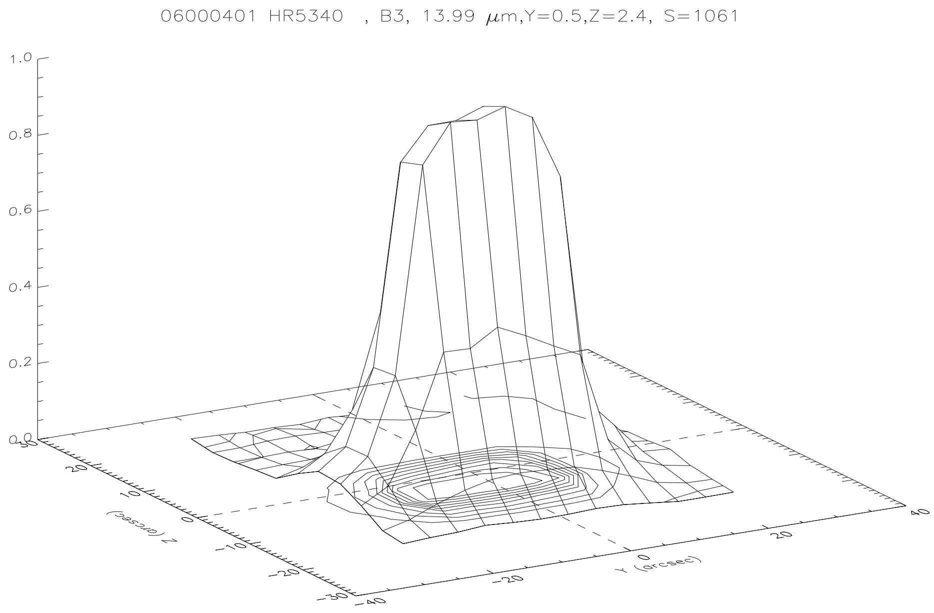

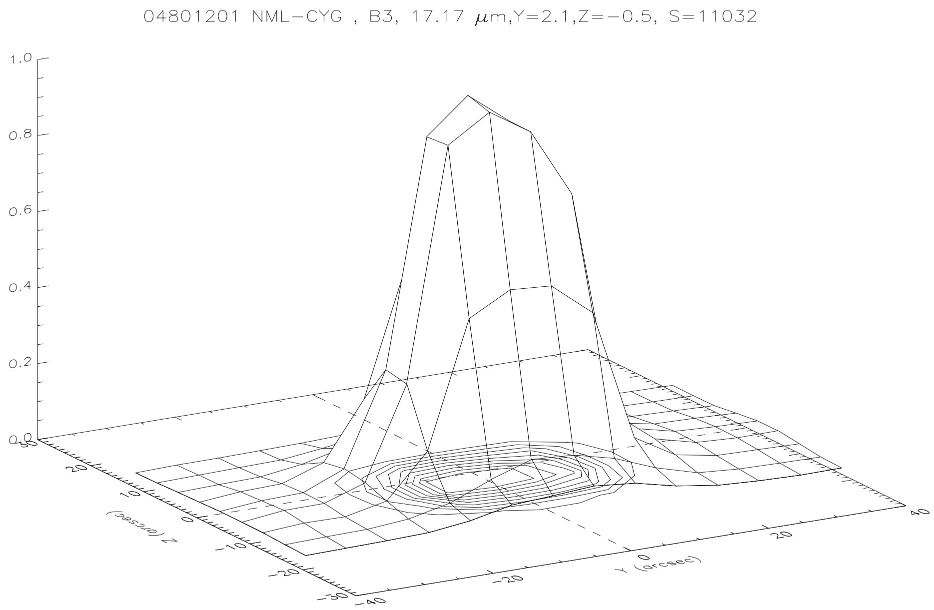

Figure 7: Beam profiles for Band 3, normalised to the maximum signal, given in the plot title (in μV/s). Contour plots are in steps of 10%, starting at 90% from the peak signal. The profiles have been shifted by the Y,Z offsets indicated, as provided by the pointing reconstruction algorithm (OLP Version $\geq$ 6.1)

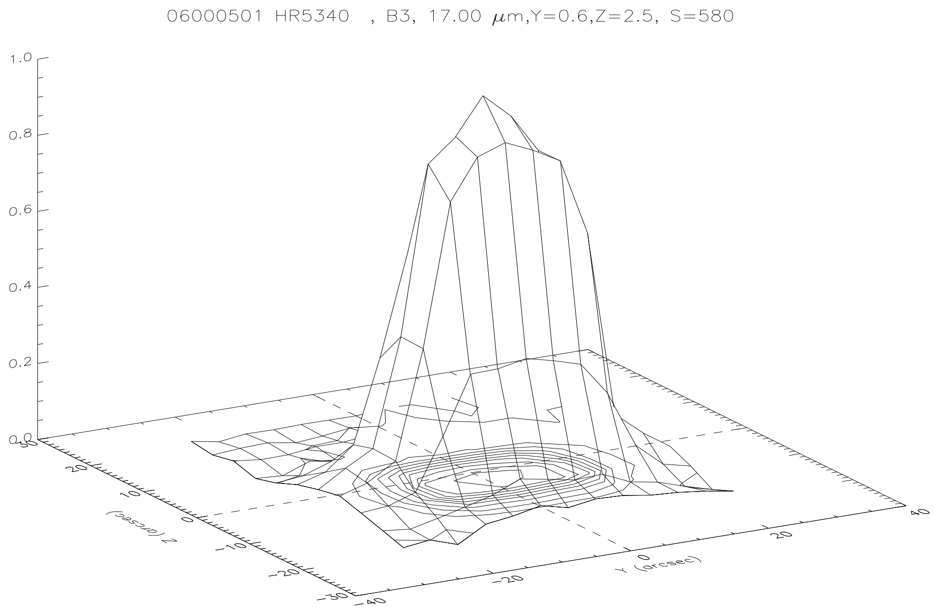

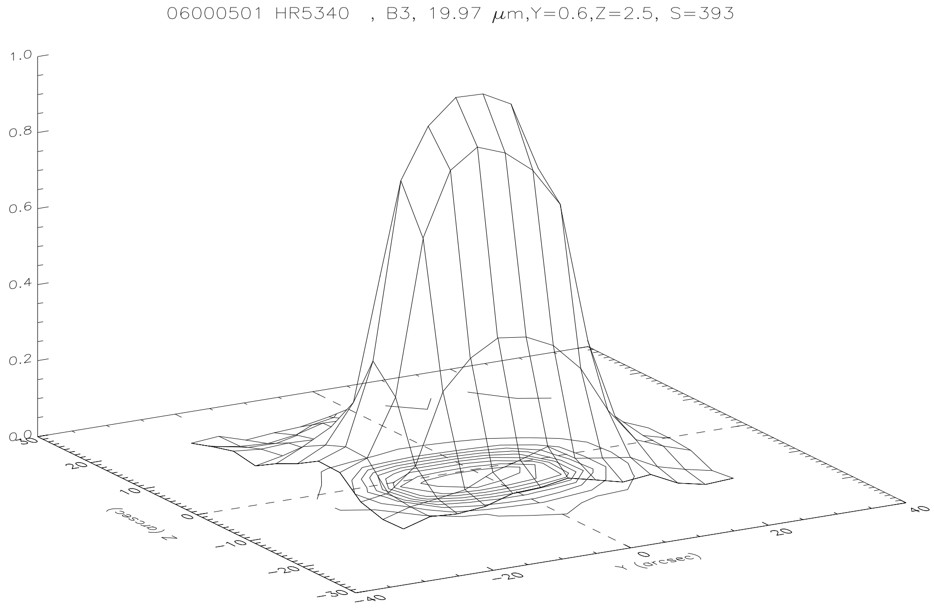

Figure 8: Beam profiles for Band 3, normalised to the maximum signal, given in the plot title (in μV/s). Contour plots are in steps of 10%, starting at 90% from the peak signal. The profiles have been shifted by the Y,Z offsets indicated, as provided by the pointing reconstruction algorithm (OLP Version $\geq$ 6.1)

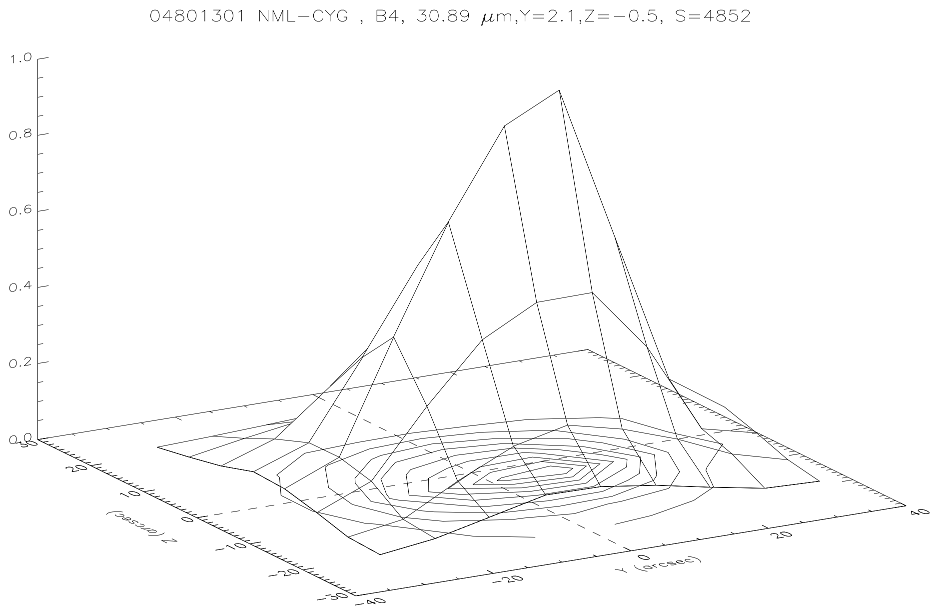

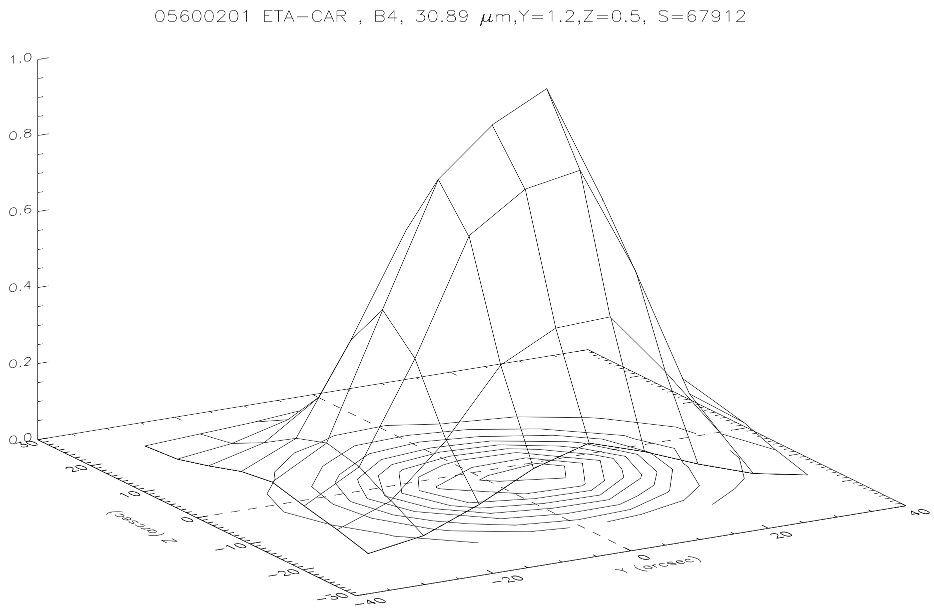

Figure 9: Beam profiles for Band 4, normalised to the maximum signal, given in the plot title (in μV/s). Contour plots are in steps of 10%, starting at 90% from the peak signal. The profiles have been shifted by the Y,Z offsets indicated, as provided by the pointing reconstruction algorithm (OLP Version $\geq$ 6.1)

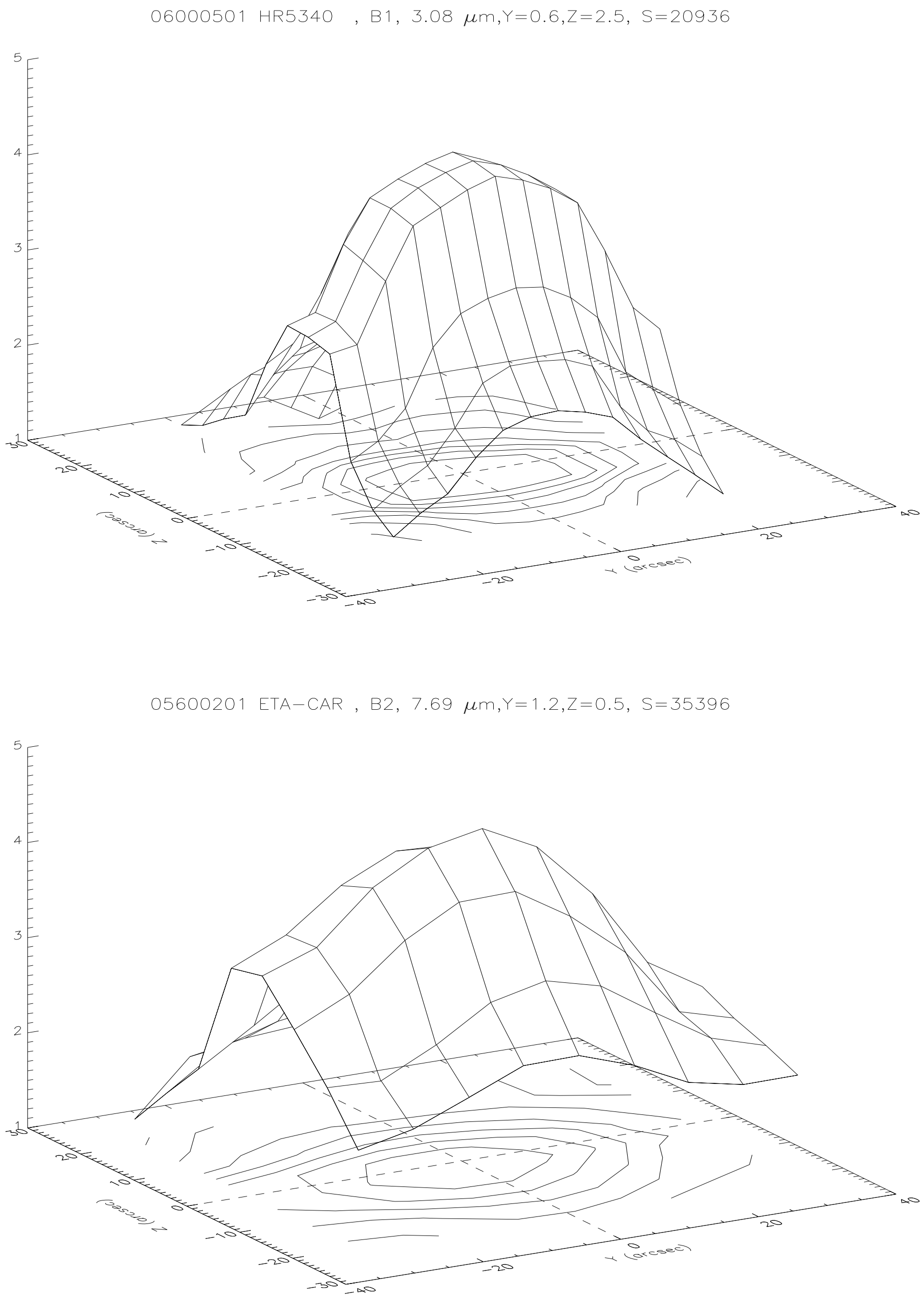

Figure 10: Beam profiles for Bands 1 and 2, in absolute signal values, on a LOG10 scale. The maximum signal is given in the plot title (in μV/s). Contour plots are in steps of 10%, starting at 90% from the LOG10 of the peak signal. The profiles have been shifted by the Y,Z offsets indicated, as provided by the pointing reconstruction algorithm (OLP Version $\geq$ 6.1)

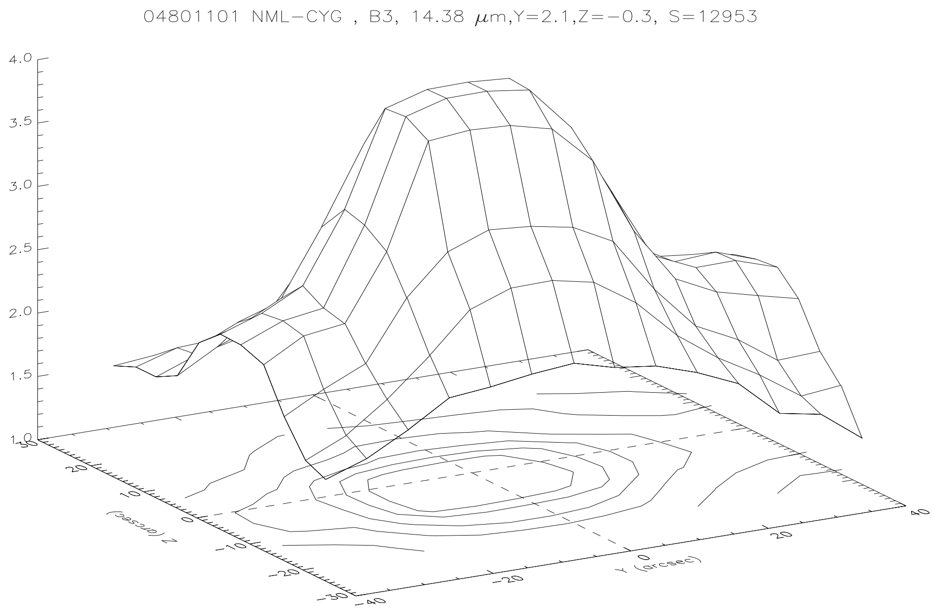

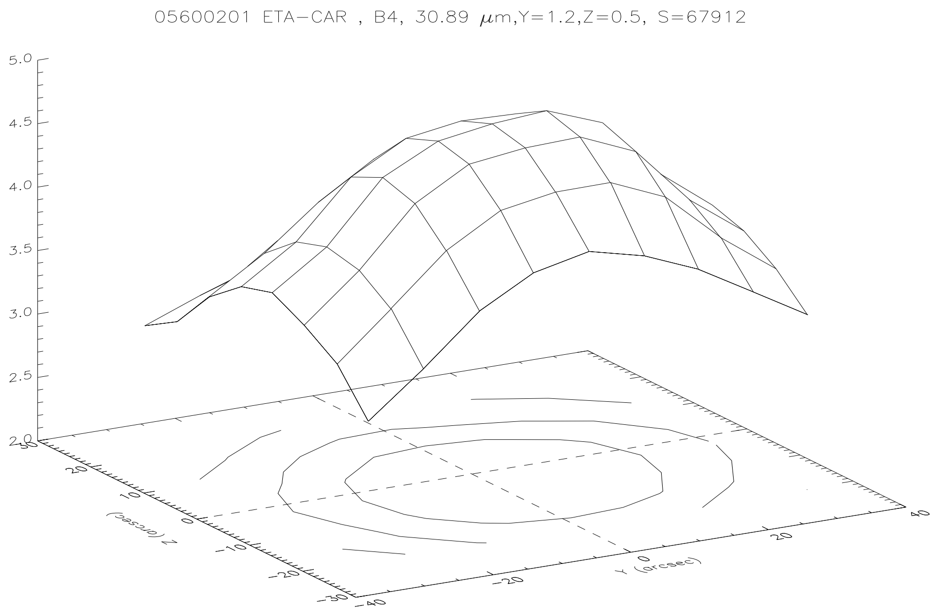

Figure 11: Beam profiles for Bands 3,4, in absolute signal values, on a LOG10 scale. The maximum signal is given in the plot title (in μV/s). Contour plots are in steps of 10%, starting at 90% from the LOG10 of the peak signal. The profiles have been shifted by the Y,Z offsets indicated, as provided by the pointing reconstruction algorithm (OLP Version $\geq$ 6.1)

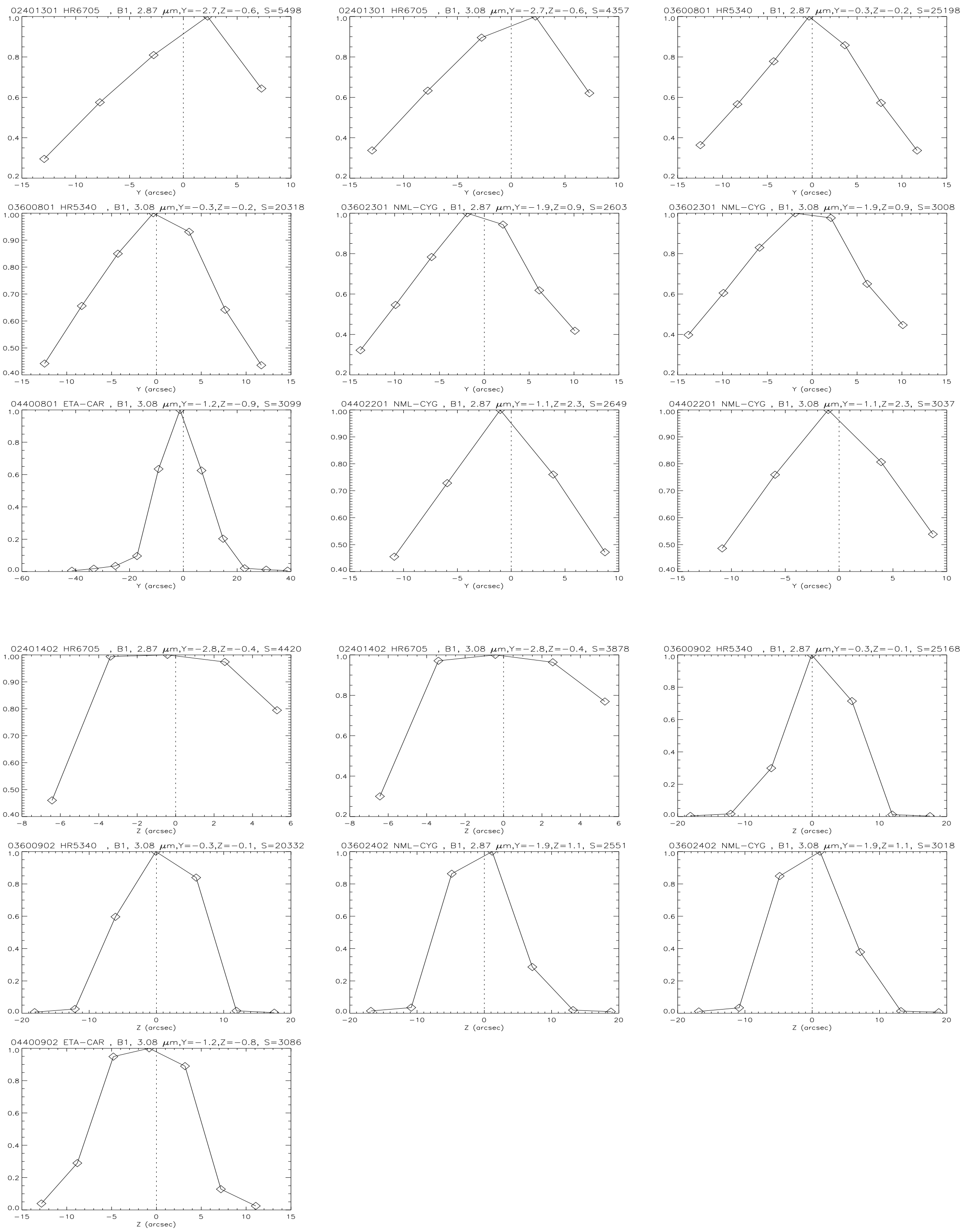

Figure 12: Y (*TOP*) and Z (*BOTTOM*) profiles for Band 1, obtained in the PV FPG-verification "cross" rasters.

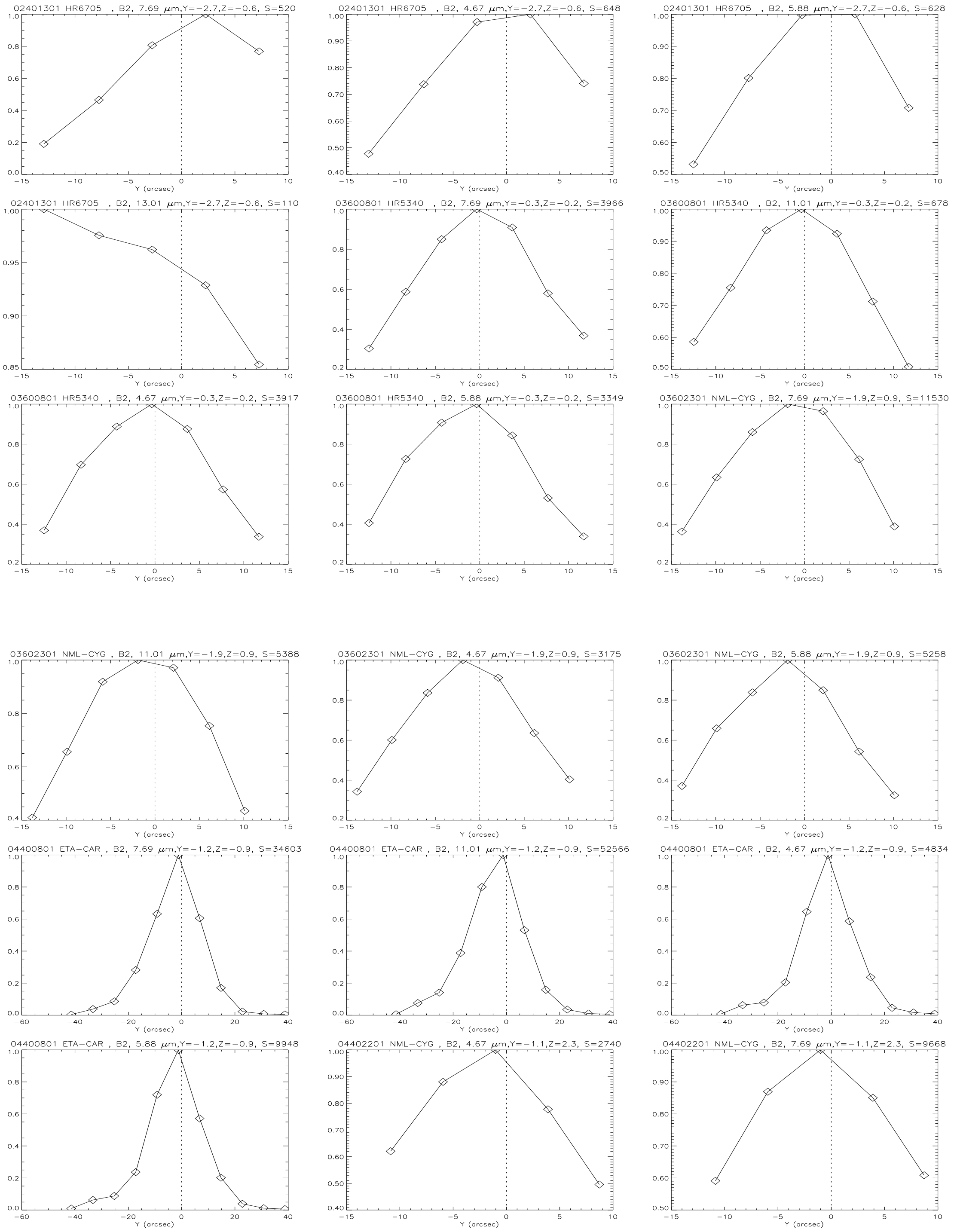

Figure 13: Y profiles for Band 2, obtained in the PV FPG-verification "cross" rasters.

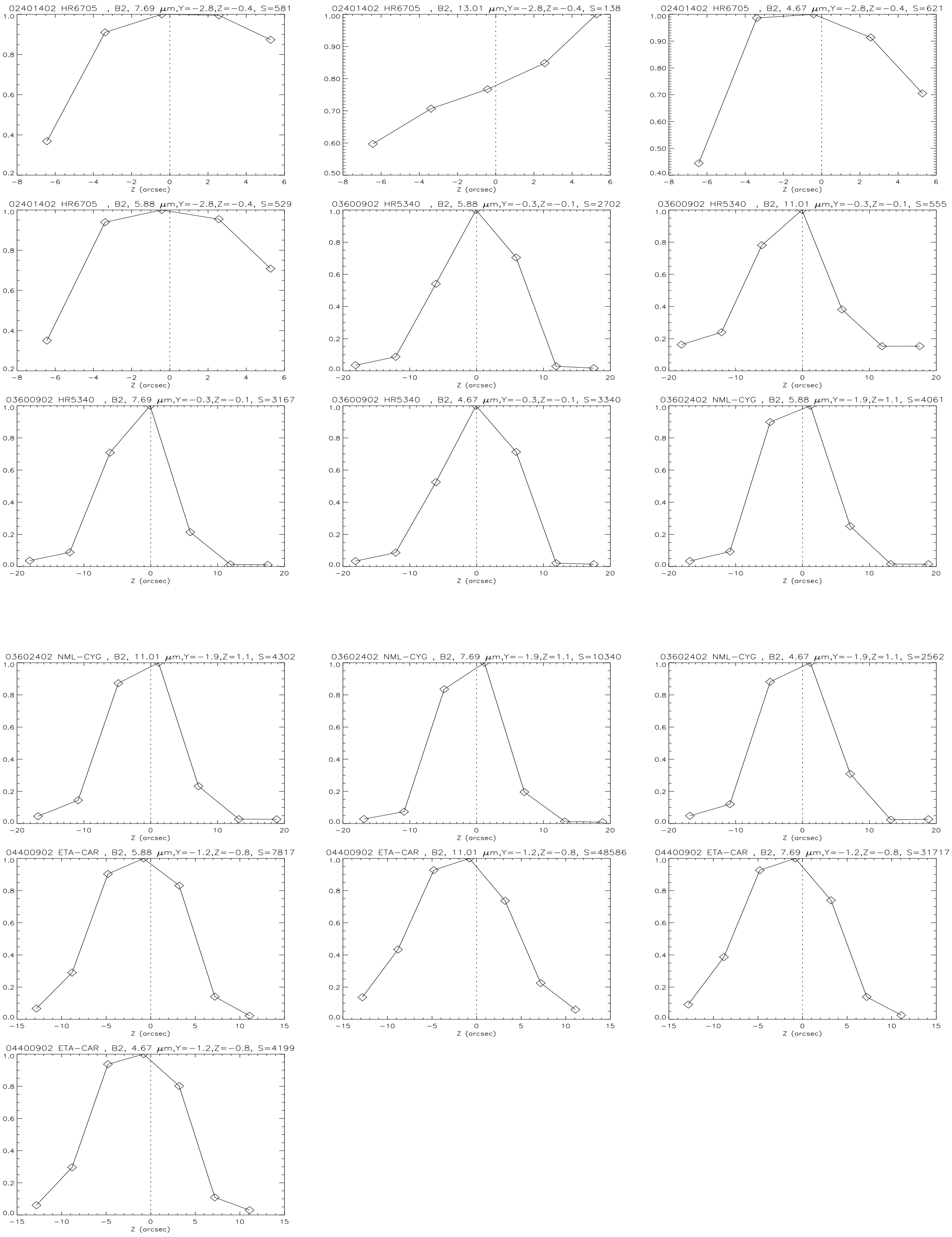

Figure 14: Z profiles for Band 2, obtained in the PV FPG-verification "cross" rasters.

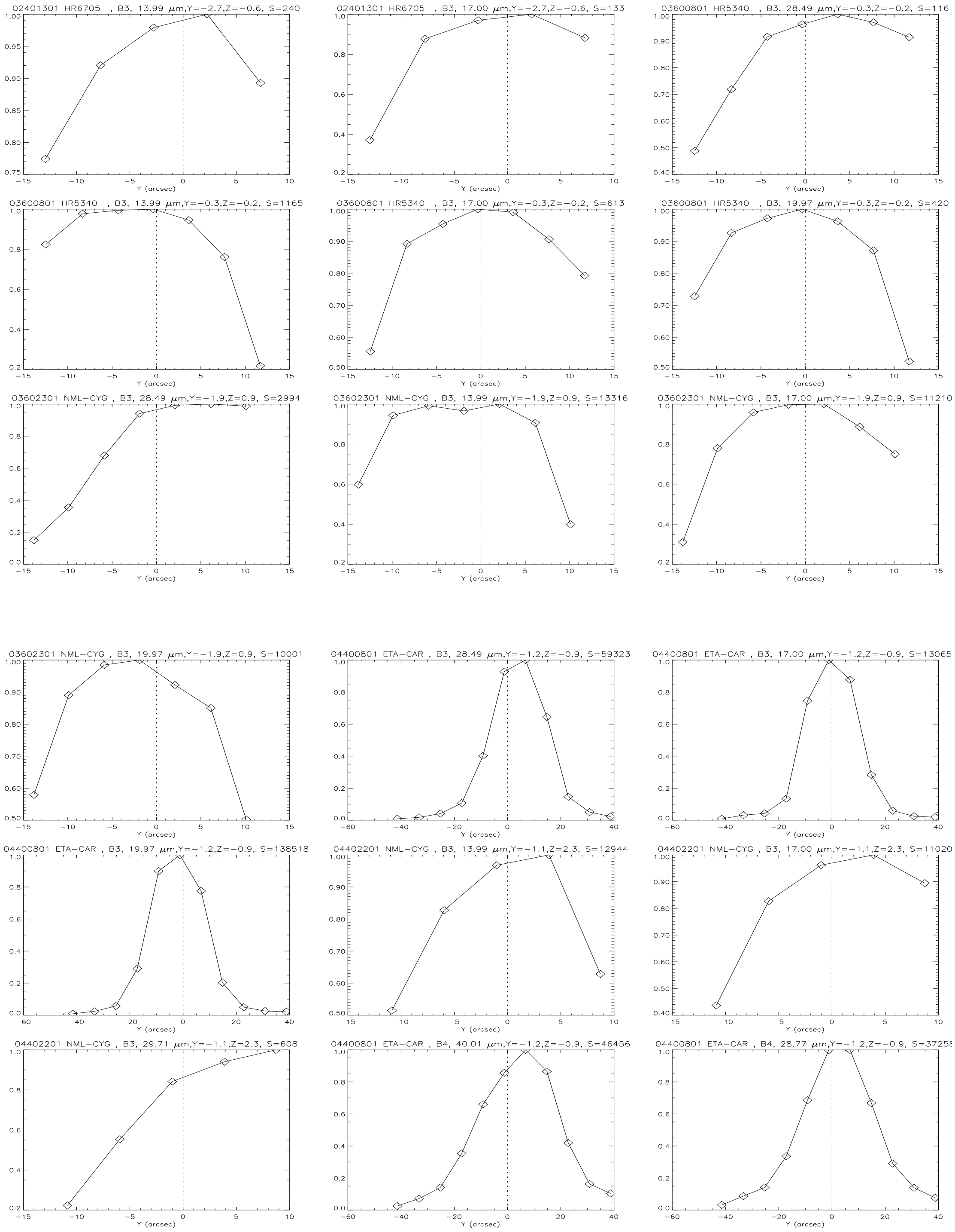

Figure 15: Y profiles for Band 2, obtained in the PV FPG-verification "cross" rasters.

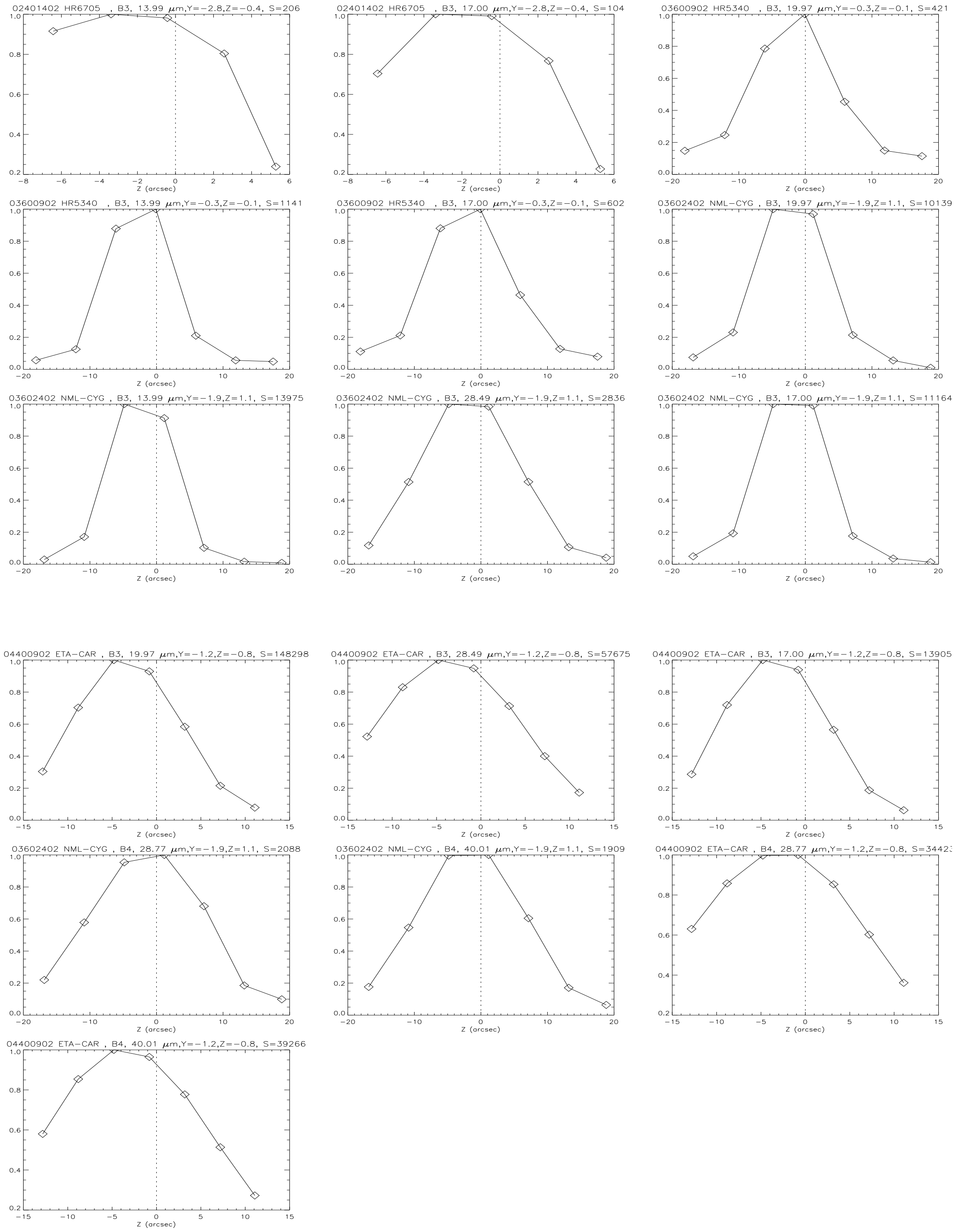

Figure 16: Z profiles for Bands 3 and 4, obtained in the PV FPG-verification "cross" rasters.

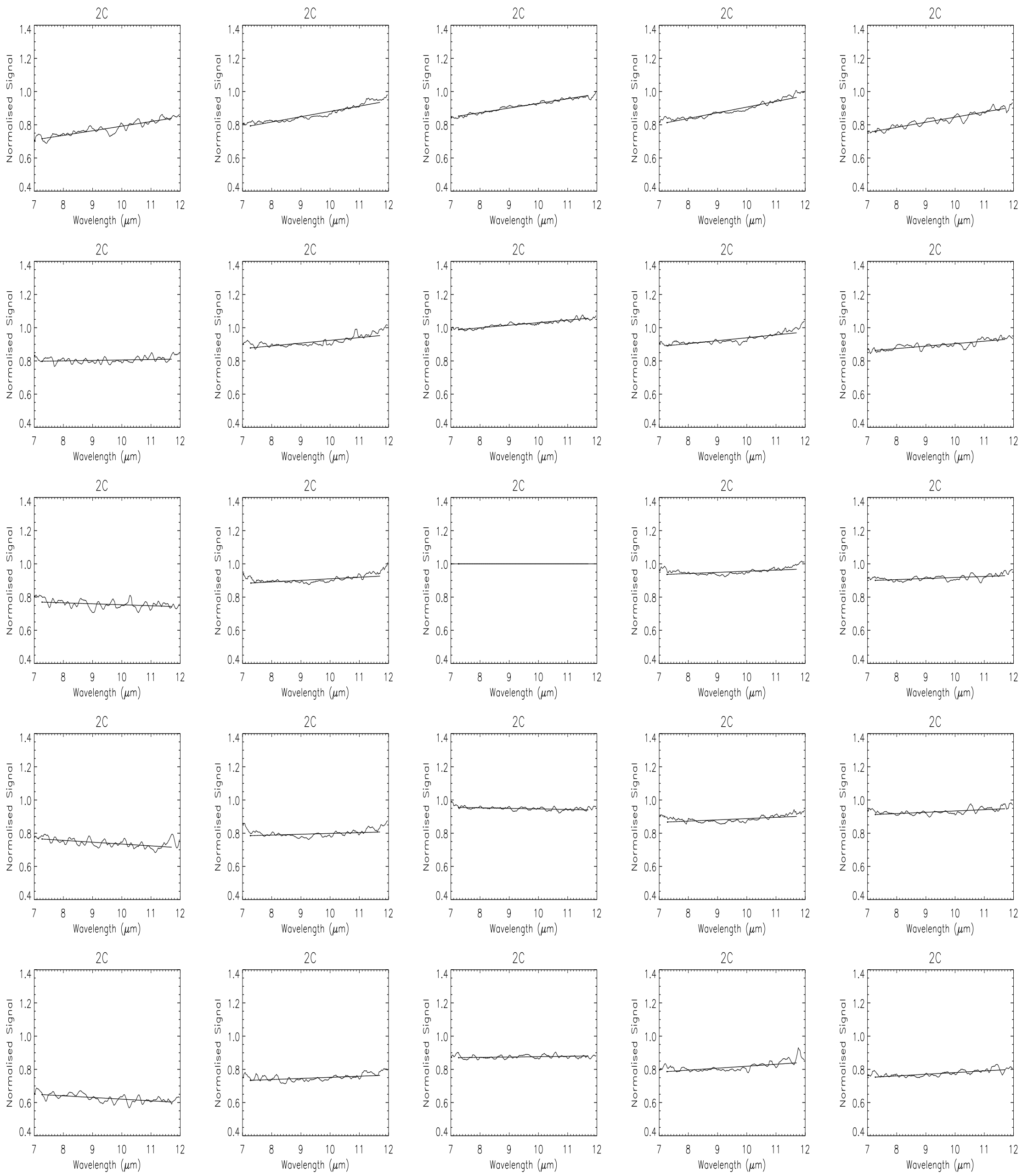

Figure 17: Wavelength dependance of the beam profile across AOT band 2C, obtained from the REV 640 AOT1-like 5X5 raster centred on HR5340. Each box shows the ratio of the spectrum to the centre position. Each box correspond to one raster point, separated by the adiacent ones by 2 arcseconds. Y increases from left to right and Z increases from top to bottom.

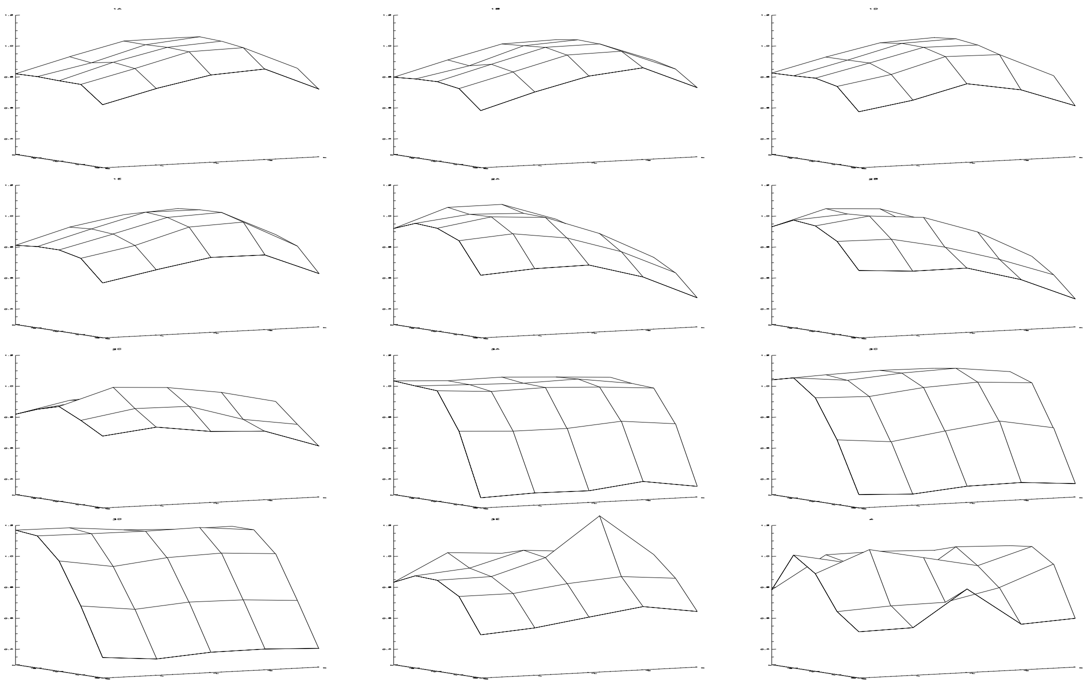

Figure 18: The top (+/- 4 arcsecond box) of the beam profiles for each grating AOT band is shown as resulting from the average signal across each AOT band of the 5X5 CUS raster experiment on HR5340 performed in REV 640. The profiles are normalised to the centre position, corresponding to HR5340 itself. The AOT bands go in increasing wavelengths from left to right and from top to bottom. The s/c Y-axis increases from -4 arcsec to 4 arcseconds in steps of 2 arcseconds from left to right. The s/c Z-axis increases from -4 arcsec to 4 arcseconds in steps of 2 arcseconds in the direction towards the plot. The normalised vertical scale goes from 0.3 to 1.2 in steps of 0.2. The top of the profile appears to depend mainly on the detector band used, and not on the aperture used, confirming the FPG calibration.

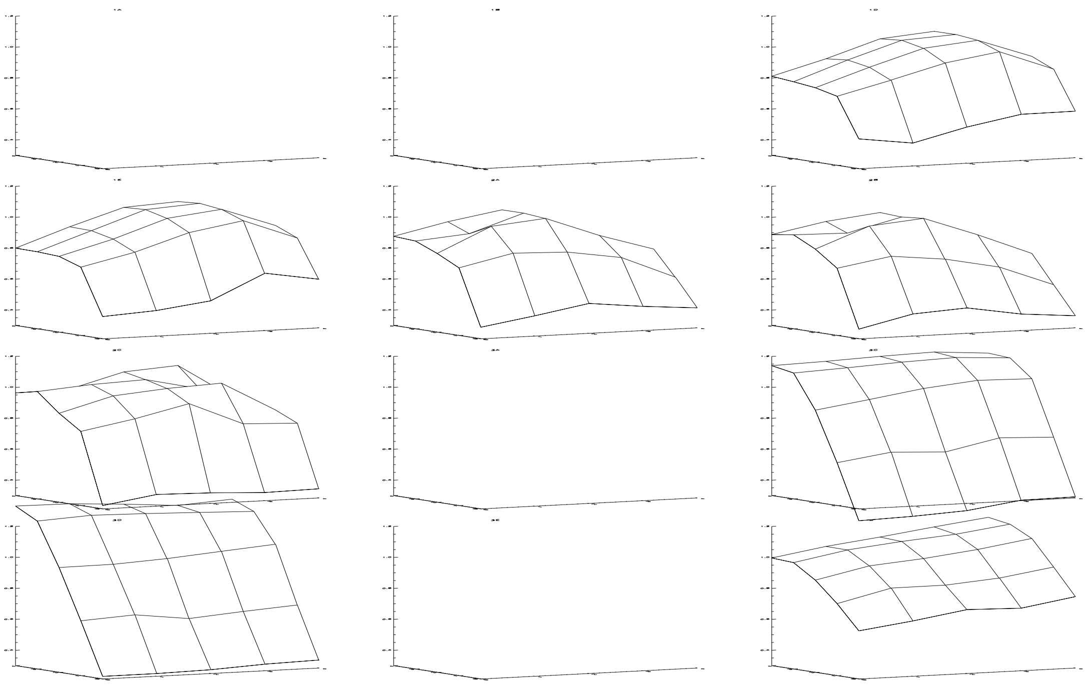

Figure 19: The top (+/- 4 arcsecond box) of the beam profiles for grating AOT bands is shown as resulting from the average signal across each AOT band of the 5X5 CUS raster experiment on NML-CYG, performed in REV 742. The profiles are normalised to the centre position, corresponding to HR5340 itself. The AOT bands go in increasing wavelengths from left to right and from top to bottom. The s/c Y-axis increases from -4 arcsec to 4 arcseconds in steps of 2 arcseconds from left to right. The s/c Z-axis increases from -4 arcsec to 4 arcseconds in steps of 2 arcseconds in the direction towards the plot. The normalised vertical scale goes from 0.3 to 1.2 in steps of 0.2. The FP band data still need to be reduced. Aperture 2,3 and 4 were used for this experiment, so the AOT bands making use of Aperture 1 do not appear. Profiles are very similar to the ones obtained on HR5340.

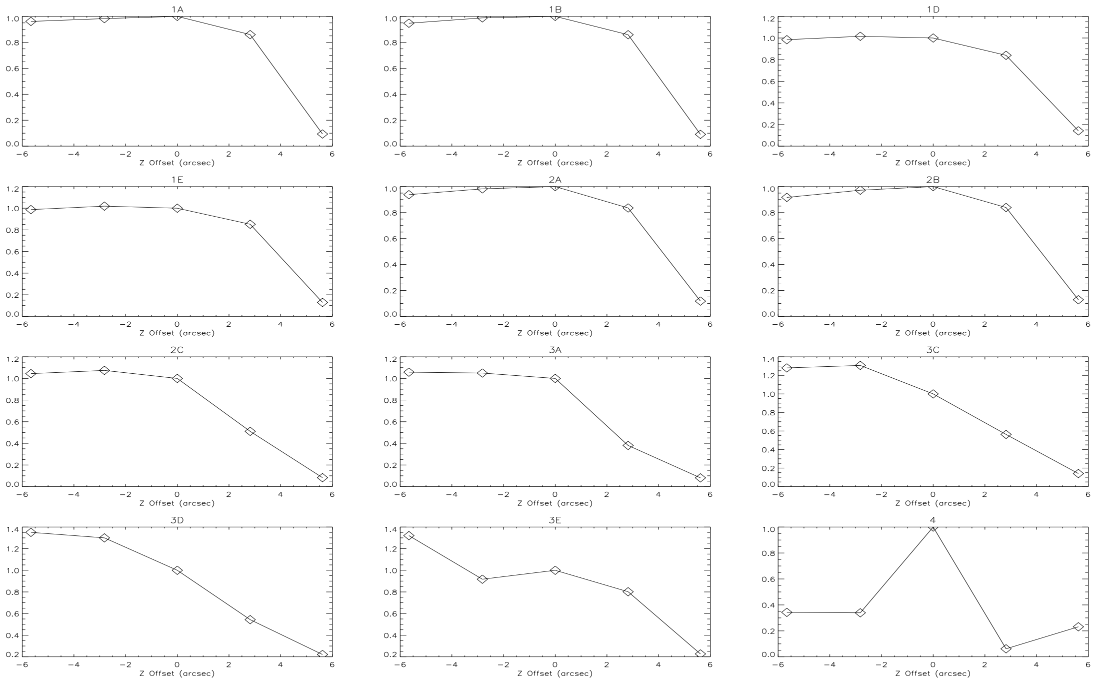

Figure 20: Beam profiles along the Z axis for each grating AOT band as resulting by averaging the signals over each AOT band from the AOT1's map performed on HR6705 in REV126.

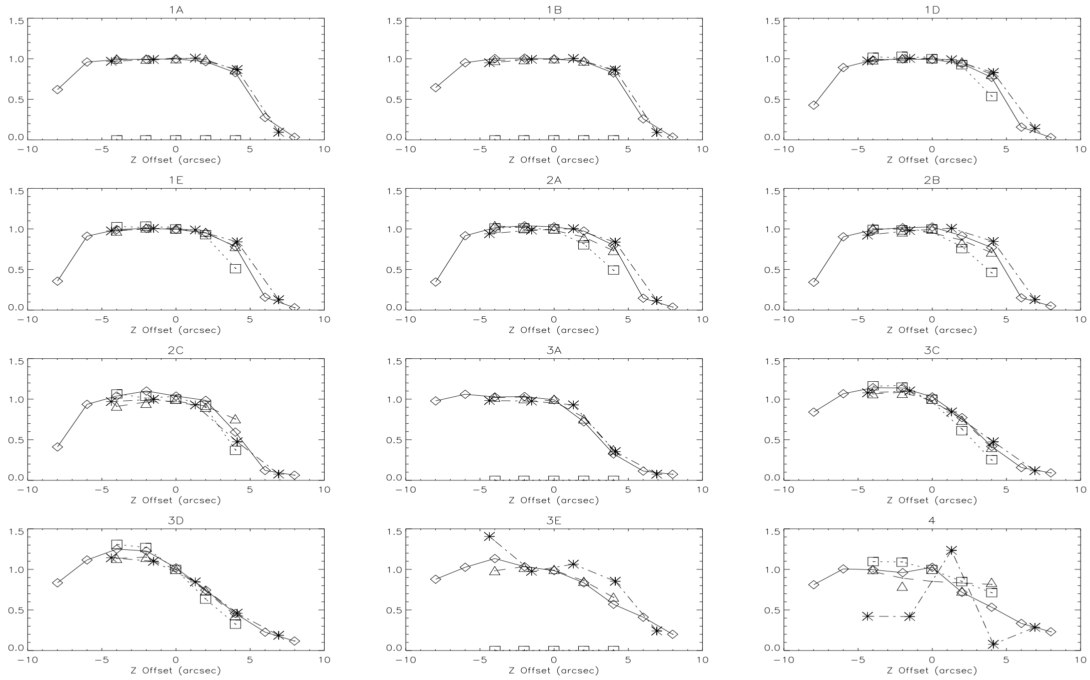

Figure 21: Beam profiles along the Z-axis obtained by various AOT1 (like) exercises are shown here. The HR6705 data are represnted by asterisks, the HR5340 data by triangles, the NML-CYG data by squares. The data obtained with the raster done on HR1457 in REV 860 is shown with romboids. The agreement between these different data sets is promising. Only the REV126 HR6705 data set has been shifted by the known pointing offset of 1.3 arcsecond.

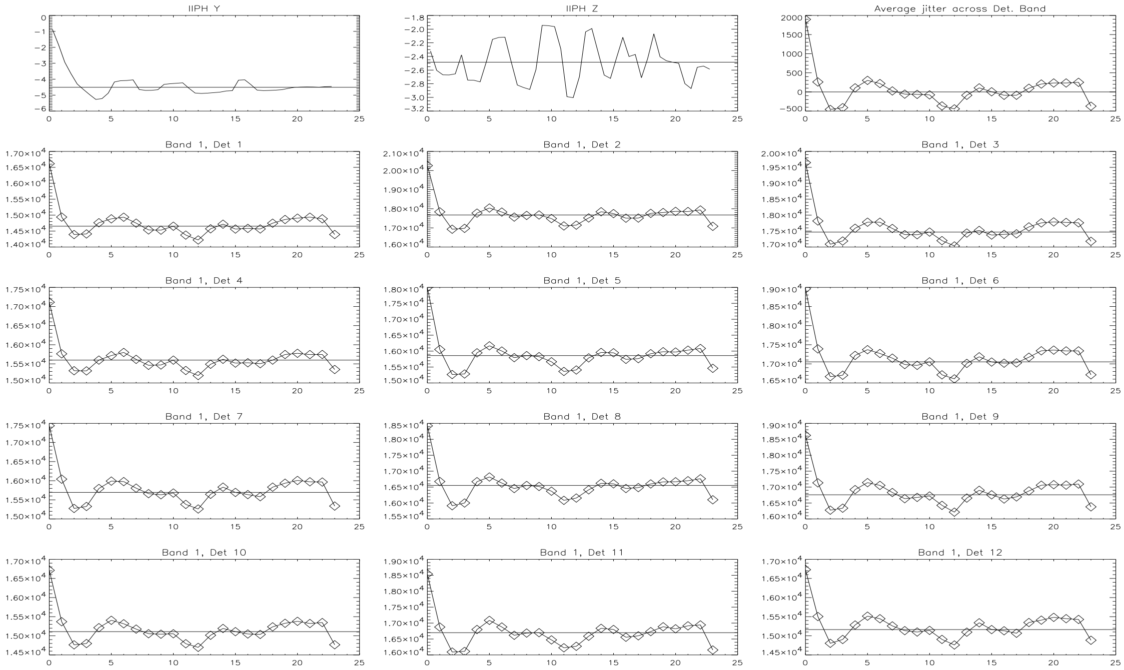

Figure 22: Pointing jitter induced correlated noise for Band 1 at 2.8 μm. Data refer to 20 seconds spent on data point m=6, n=6 of the full beam profile characterisation raster 06000401. The upper left panels shown the IIPH behaviour in Y and Z axis respectively. The upper right panel shows the average jitter across the detector band. The other panels show the time behaviour of each of the 12 element detector array signals.

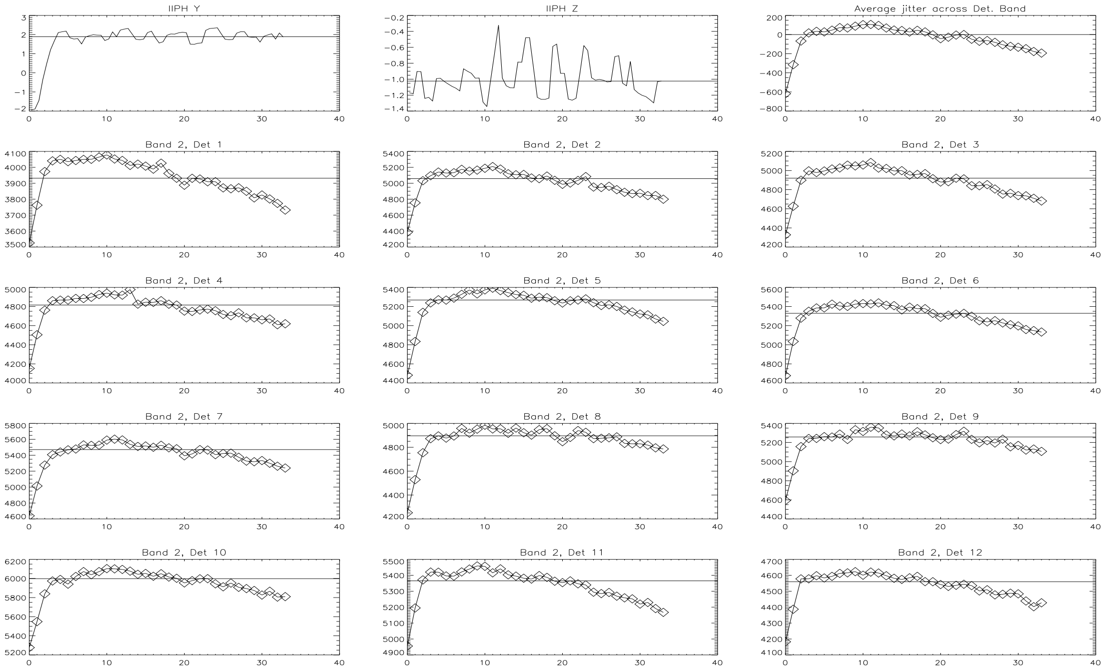

Figure 23: Pointing jitter induced correlated noise for Band 2 at 5.9 μ. Data refer to 20 seconds spent on data point m=4, n=1 of the beam profile cross-raster 03602301. The upper left panels shown the IIPH behaviour in Y and Z axis respectively. The upper right panel shows the average jitter across the detector band. The other panels show the time behaviour of each of the 12 element detector array signals.

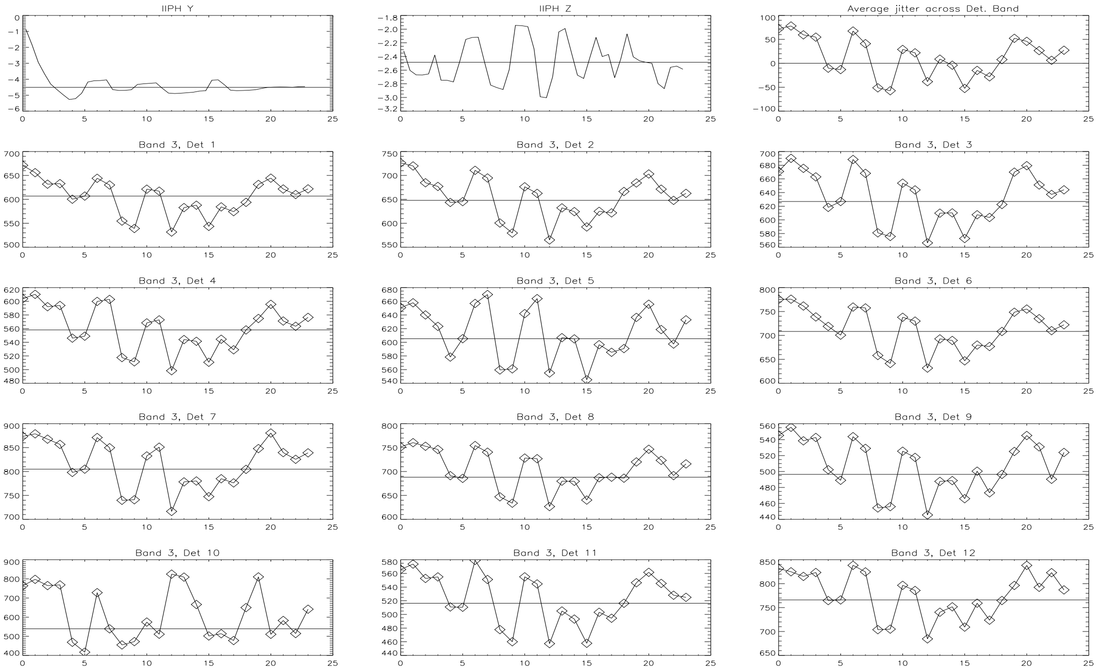

Figure 24: Pointing jitter induced correlated noise for Band 3 at 14 μm. Data refer to 20 seconds spent on data point m=6, n=6 of the full beam profile characterisation raster 06000401. The upper left panels shown the IIPH behaviour in Y and Z axis respectively. The upper right panel shows the average jitter across the detector band. The other panels show the time behaviour of each of the 12 element detector array signals.

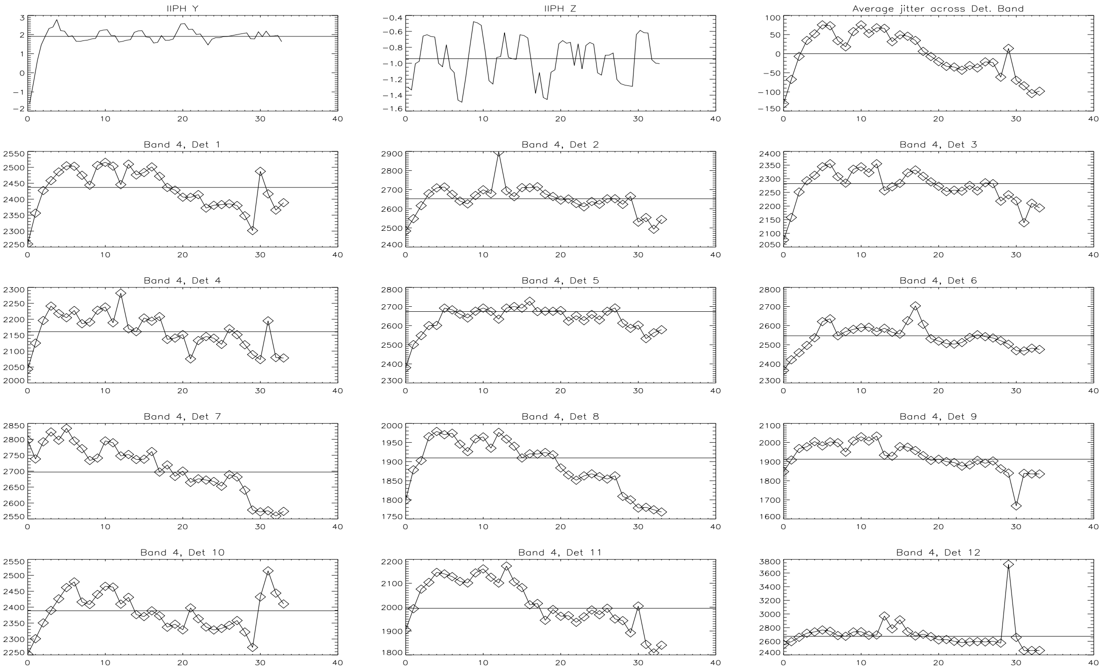

Figure 25: Pointing jitter induced correlated noise for Band 4 at 40 μm. Data refer to 20 seconds spent on data point m=4, n=1 of the beam profile cross raster 03602301. The upper left panels shown the IIPH behaviour in Y and Z axis respectively. The upper right panel shows the average jitter across the detector band. The other panels show the time behaviour of each of the 12 element detector array signals.

Appendix I: CAPs

```
{\underline CUS Rasters}
.run ISOT04$DKB100:[ASALAMA.IA.SCRIPTS]C411_RASTER.PRO

; Enter TDT number:

;-------------------------------------------------------
  tdtn='02401402'
;-------------------------------------------------------

; Read SPD and IIPH file

  iiph=read_fiiph('iiph'+tdtn+'.FITS')
  spd=read_fspd('SWSP'+tdtn+'.FITS')

; select the relevant parts of the spd

  section=0
  plot,spd.data.grpos(section),tit='Section: '+string(section)

; Enter one data point per section as a vector of indexes

;------------------------------------------------------
  ndat=[2000,5000]
;------------------------------------------------------

; Process the spd, i.e.
; derive a beam profile structure and store it in a .xdr file

  c411_raster, spd, iiph, ndat

; After processing a number of TDTs, print the overview table 1 and
; plot surface/contour plots of the beamprofiles:

  $dir/size ISOT04$DKB300:[DATA.AS.BEAMS]BP*.xdr/out=beamlist.txt
  print_beam_table1,'beamlist.txt'
  plot_rasters_table1,'beamlist.txt'
; This will create one .ps file per plot

; View table 1:

  $ed ISOT04$DKB300:[DATA.AS.BEAMS]table1.txt

; And when you are sure you have done a good job:
; clean it up!

  $pu ISOT04$DKB300:[DATA.AS.BEAMS]
;
; All of this can also be run as a .com file once the ndat's are known:

  tdtn='02401402'
```

```
  ndat=[100,300,600,800,1000,1200]
  iiph=read_fiiph('iiph'+tdtn+'.FITS')
  spd=read_fspd('SWSP'+tdtn+'.FITS')
  c411_raster, spd, iiph, ndat

  tdtn='02401301'
  ndat=[200,500,700,900,1150]
  iiph=read_fiiph('iiph'+tdtn+'.FITS')
  spd=read_fspd('SWSP'+tdtn+'.FITS')
  c411_raster, spd, iiph, ndat


  tdtn='03600801'
  ndat=[200,500,800,1100,1400]
  iiph=read_fiiph('iiph'+tdtn+'.FITS')
  spd=read_fspd('SWSP'+tdtn+'.FITS')
  c411_raster, spd, iiph, ndat

  tdtn='03600902'
  ndat=[200,500,800,1000,1300]
  iiph=read_fiiph('iiph'+tdtn+'.FITS')
  spd=read_fspd('SWSP'+tdtn+'.FITS')
  c411_raster, spd, iiph, ndat

  tdtn='03602301'
  ndat=[200,500,900,1100,1400]
  iiph=read_fiiph('iiph'+tdtn+'.FITS')
  spd=read_fspd('SWSP'+tdtn+'.FITS')
  c411_raster, spd, iiph, ndat

  tdtn='03602402'
  ndat=[200,500,700,1000,1300]
  iiph=read_fiiph('iiph'+tdtn+'.FITS')
  spd=read_fspd('SWSP'+tdtn+'.FITS')
  c411_raster, spd, iiph, ndat

  tdtn='04003001'
  ndat=200
  iiph=read_fiiph('iiph'+tdtn+'.FITS')
  spd=read_fspd('SWSP'+tdtn+'.FITS')
  c411_raster, spd, iiph, ndat
; note this is a special case with ROLL determining
; the orientation of the raster: REDO the following?

  tdtn='04003102'
  ndat=200
  iiph=read_fiiph('iiph'+tdtn+'.FITS')
  spd=read_fspd('SWSP'+tdtn+'.FITS')
  c411_raster, spd, iiph, ndat

  tdtn='04400801'
  ndat=[300,700,1200,1600]
  iiph=read_fiiph('iiph'+tdtn+'.FITS')
```

```
spd=read_fspd('SWSP'+tdtn+'.FITS')
c411_raster, spd, iiph, ndat

tdtn='04400902'
ndat=[200,500,800,1100]
iiph=read_fiiph('iiph'+tdtn+'.FITS')
spd=read_fspd('SWSP'+tdtn+'.FITS')
c411_raster, spd, iiph, ndat

tdtn='04402201'
ndat=[200,500,700]
iiph=read_fiiph('iiph'+tdtn+'.FITS')
spd=read_fspd('SWSP'+tdtn+'.FITS')
c411_raster, spd, iiph, ndat

tdtn='04402302'
ndat=[100,400,600]
iiph=read_fiiph('iiph'+tdtn+'.FITS')
spd=read_fspd('SWSP'+tdtn+'.FITS')
c411_raster, spd, iiph, ndat

tdtn='06000401'
ndat=2000
iiph=read_fiiph('iiph'+tdtn+'.FITS')
spd=read_fspd('SWSP'+tdtn+'.FITS')
c411_raster, spd, iiph, ndat

tdtn='06000501'
ndat=[2000,5000]
iiph=read_fiiph('iiph'+tdtn+'.FITS')
spd=read_fspd('SWSP'+tdtn+'.FITS')
c411_raster, spd, iiph, ndat

tdtn='06000701'
ndat=[2000,5000]
iiph=read_fiiph('iiph'+tdtn+'.FITS')
spd=read_fspd('SWSP'+tdtn+'.FITS')
c411_raster, spd, iiph, ndat

tdtn='04801101'
ndat=1500
iiph=read_fiiph('iiph'+tdtn+'.FITS')
spd=read_fspd('SWSP'+tdtn+'.FITS')
c411_raster, spd, iiph, ndat

tdtn='04801201'
ndat=1500
iiph=read_fiiph('iiph'+tdtn+'.FITS')
spd=read_fspd('SWSP'+tdtn+'.FITS')
c411_raster, spd, iiph, ndat

tdtn='04801301'
ndat=1000
```

```
  iiph=read_fiiph('iiph'+tdtn+'.FITS')
  spd=read_fspd('SWSP'+tdtn+'.FITS')
  c411_raster, spd, iiph, ndat

  tdtn='05600201'
  ndat=1000
  iiph=read_fiiph('iiph'+tdtn+'.FITS')
  spd=read_fspd('SWSP'+tdtn+'.FITS')
  c411_raster, spd, iiph, ndat
;---------------------------------------------------------------------------

Things to plot in the EOM of the m_n plots:

02401301M3N1_2P87.PS;1 Y-jitter
03602301M4N1_13P99.PS;1 Z-jitter
03602301M4N1_40P01.PS;1 both (band 4)
03602301M4N1_4P67.PS;1 y, band 2
03602301M4N1_5P88.PS;1 y, band 2

; To plot the crosses:

;Only the Y-profiles:
; => Comment the if(m eq 1) section

set_plot,"ps"
device,/landscape
device,filename='[.beams]crosses_1_y.ps'
!p.multi=0
!p.multi=[0,3,3,0,0]
plot_rasters_table1,'beamlist.txt',1
device,/close

set_plot,"ps"
device,/landscape
device,filename='[.beams]crosses_2_y.ps'
!p.multi=0
!p.multi=[0,3,3,0,0]
plot_rasters_table1,'beamlist.txt',2
device,/close

set_plot,"ps"
device,/landscape
device,filename='[.beams]crosses_3_4_y.ps'
!p.multi=0
!p.multi=[0,3,3,0,0]
plot_rasters_table1,'beamlist.txt',3
plot_rasters_table1,'beamlist_b4_y.txt',4
device,/close

;Only the Z-profiles:
; => Comment the if(n eq 1) section

set_plot,"ps"
```

```
device,/landscape
device,filename='[.beams]crosses_1_z.ps'
!p.multi=0
!p.multi=[0,3,3,0,0]
plot_rasters_table1,'beamlist.txt',1
device,/close

set_plot,"ps"
device,/landscape
device,filename='[.beams]crosses_2_z.ps'
!p.multi=0
!p.multi=[0,3,3,0,0]
plot_rasters_table1,'beamlist.txt',2
device,/close

set_plot,"ps"
device,/landscape
device,filename='[.beams]crosses_3_4_z.ps'
!p.multi=0
!p.multi=[0,3,3,0,0]
plot_rasters_table1,'beamlist.txt',3
plot_rasters_table1,'beamlist.txt',4
device,/close

; Big rasters surface contour plots:
; edit plot_rasters_table1 and put the /ps option in the call to plot_beam

plot_rasters_table1,'beamlist.txt',1
plot_rasters_table1,'beamlist.txt',2
plot_rasters_table1,'beamlist.txt',3
plot_rasters_table1,'beamlist.txt',4
plot_rasters_table1,'beamlist.txt',5
plot_rasters_table1,'beamlist.txt',6

; to plot those on a log scale, use
plot_rasters_table1_log_surf,'beamlist.txt',1
```

AOT1 and CUS AOT1-like maps

```
; Filename: BEAM_AOTS.CAP
;
; This CAP describes how to process beam profile calibrations obtained via
; AOTs and AOT-like COIFs.
; Input: SPDs and IIPHs
; Output: Beam profile structure
;
; AOT-like COIFs:

; HR5340
; This is a set of three TDTs, each one associated with an m X n raster,
; and one aperture (1,2,3)
; For each SPD,
; decompose it in an m X n array of SPDs.
; First ensure all of these have the same number of points.
; The first one will in general have more data points (initial overhead)
; these will have to be discarded
; Take the latest set of CAL files (OLP V7.0)
  cs
  .run ISOT04$DKB100:[ASALAMA.IA.SCRIPTS]cleanstruct
; Read spd
  spd=read_fspd('swsp64000101.fits')
;  HR5340_split_prepare,spd

; Create an m X n array of spds
  HR5340_SPLIT_APER1,spd,spds

; Derive AARs, also as an m X n array of AARs
  cus_aot1_DAAR, spds, aars

; Process now these AARs, (sigclip/flatfield) and rebin to a resolution of 100.
; The wavelength scale is taken to be the one defined by point m=1,n=1.
  cus_aot1_daarb,aars,aarsb1
  save,/xdr,filename='ISOT04$DKB300:[DATA.AS]HR5340_aper1.aarsb',aarsb1

; Do similarly for the other two apertures:

  spd=read_fspd('swsp64000202.fits')
;  HR5340_split_prepare,spd
  HR5340_SPLIT_APER2,spd,spds
  cus_aot1_DAAR, spds, aars
  cus_aot1_daarb,aars,aarsb2
  save,/xdr,filename='ISOT04$DKB300:[DATA.AS]HR5340_aper2.aarsb',aarsb2

  spd=read_fspd('swsp64000303.fits')
;  HR5340_split_prepare,spd
  HR5340_SPLIT_APER3,spd,spds
  cus_aot1_DAAR, spds, aars
  cus_aot1_daarb,aars,aarsb3
  save,/xdr,filename='ISOT04$DKB300:[DATA.AS]HR5340_aper3.aarsb',aarsb3
```

```
; Derive for each AOT Band average fluxes and first order polynome fits
  across the AOT band:
;
  HR5340_plot_all,allfit,allave
  HR5340_plot_all,allfit,allave,/plotonly,/surface

; Put these into a .ps file:

  set_plot,"ps"
  device,/landscape
  device,filename='ISOT04$DKB300:[DATA.AS.BEAMS]HR5430_CUSAOT1.ps'
  HR5340_plot_all,allfit,allave,/surface
  device,/close
  set_plot,"x"

; Store these results into a structure:

  iiph1=read_fiiph('iiph64000101.fits')
  raster_get_y_z,iiph1,y1,z1
  iiph2=read_fiiph('iiph64000202.fits')
  raster_get_y_z,iiph2,y2,z2
  iiph3=read_fiiph('iiph64000303.fits')
  raster_get_y_z,iiph3,y3,z3
  beam_obs=cusaot1_fill_beam_structure(allfit,allave,y1,z1,y2,z2,y3,z3)
  save,/xdr,filename='BP_HR5340.XDR',beam_obs

; plot the Z-profiles only

  restore,'BP_HR5340.XDR'
  set_plot,"ps"
  device,/landscape
  device,filename='ISOT04$DKB300:[DATA.AS.BEAMS]HR5340_AOT1s_Z.ps'
  hr5340_plot_zprofiles,beam_obs
  device,/close
  set_plot,"x"

; ------------------------------------------------------------------------
; NMLCYG
; This is a set of three TDTs, each one associated with an m X n raster,
; and one aperture (2,3,4)
; For each SPD,
; decompose it in an m X n array of SPDs.
; First ensure all of these have the same number of points.
; The first one will in general have more data points (initial overhead)
; these will have to be discarded
; Take the latest set of CAL files (OLP V7.0)
  cs
  .run ISOT04$DKB100:[ASALAMA.IA.SCRIPTS]cleanstruct
; Read spd
  spd=read_fspd('swsp74200101.fits')
;  NMLCYG_split_prepare,spd

; Create an m X n array of spds
```

```
  NMLCYG_SPLIT_APER2,spd,spds

; Derive AARs, also as an m X n array of AARs
  cus_aot1_DAAR, spds, aars

; Process now these AARs, (sigclip/flatfield) and rebin to a resolution of 100.
; The wavelength scale is taken to be the one defined by point m=1,n=1.
  cus_aot1_daarb,aars,aarsb2
  save,/xdr,filename='ISOT04$DKB300:[DATA.AS]NMLCYG_aper2.aarsb',aarsb2

; Do similarly for the other two apertures:

  spd=read_fspd('swsp74200202.fits')
;  NMLCYG_split_prepare,spd
  NMLCYG_SPLIT_APER3,spd,spds
  cus_aot1_DAAR, spds, aars
  cus_aot1_daarb,aars,aarsb3
  save,/xdr,filename='ISOT04$DKB300:[DATA.AS]NMLCYG_aper3.aarsb',aarsb3

  spd=read_fspd('swsp74200303.fits')
;  NMLCYG_split_prepare,spd
  NMLCYG_SPLIT_APER4,spd,spds
  cus_aot1_DAAR, spds, aars
  cus_aot1_daarb,aars,aarsb4
  save,/xdr,filename='ISOT04$DKB300:[DATA.AS]NMLCYG_aper4.aarsb',aarsb4

; Derive for each AOT Band average fluxes and first order polynome fits:
;
  NMLCYG_plot_all,allfit,allave
  NMLCYG_plot_all,allfit,allave,/plotonly,/surface

; Put these into a .ps file:

  set_plot,"ps"
  device,/landscape
  device,filename='ISOT04$DKB300:[DATA.AS.BEAMS]NMLCYG_CUSAOT1.ps'
  NMLCYG_plot_all,allfit,allave,/surface
  device,/close
  set_plot,"x"

; Store these results into a structure:

  iiph2=read_fiiph('iiph74200101.fits')
  raster_get_y_z,iiph2,y2,z2
  iiph3=read_fiiph('iiph74200202.fits')
  raster_get_y_z,iiph3,y3,z3
  beam_obs=cusaot1_fill_beam_structure(allfit,allave,y2,z2,y2,z2,y3,z3)
  save,/xdr,filename='BP_NMLCYG.XDR',beam_obs

; HR1457
; This is a set of three TDTs, each one associated with an m X n raster,
; and one aperture (1,2,3)
; For each SPD,
```

```
; decompose it in an m X n array of SPDs.
; First ensure all of these have the same number of points.
; The first one will in general have more data points (initial overhead)
; these will have to be discarded
; Take the latest set of CAL files (OLP V7.0)
  cs
  .run ISOT04$DKB100:[ASALAMA.IA.SCRIPTS]cleanstruct
; Read spd
  spd=read_fspd('swsp86002401.fits')
;  HR1457_split_prepare,spd

; Create an m X n array of spds
  HR1457_SPLIT_APER1,spd,spds

; Derive AARs, also as an m X n array of AARs
  cus_aot1_DAAR, spds, aars

; Process now these AARs, (sigclip/flatfield) and rebin to a resolution of 100.
; The wavelength scale is taken to be the one defined by point m=1,n=1.
  cus_aot1_daarb,aars,aarsb1
  save,/xdr,filename='ISOT04$DKB300:[DATA.AS]HR1457_aper1.aarsb',aarsb1

; Do similarly for the other two apertures:

  spd=read_fspd('swsp86002502.fits')
;  HR1457_split_prepare,spd
  HR1457_SPLIT_APER2,spd,spds
  cus_aot1_DAAR, spds, aars
  cus_aot1_daarb,aars,aarsb2
  save,/xdr,filename='ISOT04$DKB300:[DATA.AS]HR1457_aper2.aarsb',aarsb2

  spd=read_fspd('swsp86002603.fits')
;  HR1457_split_prepare,spd
  HR1457_SPLIT_APER3,spd,spds
  cus_aot1_DAAR, spds, aars
  cus_aot1_daarb,aars,aarsb3
  save,/xdr,filename='ISOT04$DKB300:[DATA.AS]HR1457_aper3.aarsb',aarsb3

; Derive for each AOT Band average fluxes and first order polynome fits:
;
  HR1457_plot_all,allfit,allave
  HR1457_plot_all,allfit,allave,/plotonly,/surface
; Put these into a .ps file:

;  set_plot,"ps"
;  device,/landscape
;  device,filename='ISOT04$DKB300:[DATA.AS.BEAMS]HR1457_CUSAOT1.ps'
;  HR1457_plot_all,allfit,allave,/surface
;  device,/close
;  set_plot,"x"

; Store these results into a structure:
```

```
  iiph1=read_fiiph('iiph86002401.fits')
  raster_get_y_z,iiph1,y1,z1
  iiph2=read_fiiph('iiph86002502.fits')
  raster_get_y_z,iiph2,y2,z2
  iiph3=read_fiiph('iiph86002603.fits')
  raster_get_y_z,iiph3,y3,z3
  beam_obs=cusaot1_fill_beam_structure(allfit,allave,y1,z1,y2,z2,y3,z3)
  save,/xdr,filename='BP_HR1457.XDR',beam_obs

; plot the Z-profiles only

  set_plot,"ps"
  device,/landscape
  device,filename='ISOT04$DKB300:[DATA.AS.BEAMS]HR1457_cus_AOT1s_Z.ps'
  hr1457_plot_zprofiles_avg,beam_obs
  device,/close
  set_plot,"X"
;-------------------------------------------------------------------------------
; AOTs maps:

; HR6705
; This is a set of 7 TDTs, each one is an AOT1 speed 1, done respectively at
; Y=0 Z=-6,-3,0,3,6 and Y=-6,Z=0 and Y=6,Z=0
;
; Adapt this set to work using the CUSAOT1 raster routines:
; Create an array of 1X7 SPDs
; Take the latest set of CAL files (OLP V7.0)
  cs
  .run ISOT04$DKB100:[ASALAMA.IA.SCRIPTS]cleanstruct
; Read spds
  spd=read_fspd('SWSP12601315.FITS')
  spds=replicate(spd,1,7)
  spds(0,0)=spd
  spd=read_fspd('SWSP12601117.FITS')
  spds(0,1).header=spd.header
  spds(0,1).data=spd.data
  spd=read_fspd('SWSP12601216.FITS')
  spds(0,2).header=spd.header
  spds(0,2).data=spd.data
  spd=read_fspd('SWSP12601418.FITS')
  spds(0,3).header=spd.header
  spds(0,3).data=spd.data
  spd=read_fspd('SWSP12601519.FITS')
  spds(0,4).header=spd.header
  spds(0,4).data=spd.data
  spd=read_fspd('SWSP12601620.FITS')
  spds(0,5).header=spd.header
  spds(0,5).data=spd.data
  spd=read_fspd('SWSP12601721.FITS')
  spds(0,6).header=spd.header
  spds(0,6).data=spd.data

; derive aars:
```

```
  cus_aot1_daar,spds,aars

; Process now these AARs, (sigclip/flatfield) and rebin to a resolution of 100.
; The wavelength scale is taken to be the one defined by point m=1,n=1.
  cus_aot1_daarb,aars,aarsb
  save,/xdr,filename='ISOT04$DKB300:[DATA.AS]HR6705.aarsb',aarsb

; Derive for each AOT Band average fluxes and first order polynome fits:
;
  HR6705_plot_all,allfit,allave

; Put these into a .ps file!
  set_plot,"ps"
  device,/landscape
  device,filename='ISOT04$DKB300:[DATA.AS.BEAMS]HR6705_aot1_aotbands.ps'
  HR6705_plot_all,allfit,allave
  device,/close
  set_plot,"x"

;  assign Y,Z offsets w.r.t. the HR6705 position (spd(0,0)) to each AOT

  hr6705_assign_y_z,spds,y,z

; Store these results into a structure:

  beam_obs=aot1_fill_beam_structure(allfit,allave,y,z)
  save,/xdr,filename='BP_HR6705.XDR',beam_obs

; plot the Z-profiles only

  set_plot,"ps"
  device,/landscape
  device,filename='ISOT04$DKB300:[DATA.AS.BEAMS]HR6705_AOT1s_Z.ps'
  hr6705_plot_zprofiles,beam_obs
  device,/close
  set_plot,"x"

; The Reconstructed pointing algorithm gives:

  get_offsets,'SWSP12601315.FITS',y_off,z_off & print,y_off,z_off
  get_offsets,'SWSP12601216.FITS',y_off,z_off & print,y_off,z_off
  get_offsets,'SWSP12601117.FITS',y_off,z_off & print,y_off,z_off
  get_offsets,'SWSP12601418.FITS',y_off,z_off & print,y_off,z_off
  get_offsets,'SWSP12601519.FITS',y_off,z_off & print,y_off,z_off
  get_offsets,'SWSP12601620.FITS',y_off,z_off & print,y_off,z_off
  get_offsets,'SWSP12601721.FITS',y_off,z_off & print,y_off,z_off

; y_off ~ -0.6",     z_off ~ +1.3"
; (Offsets w.r.t. the intended pointing)
;-----------------------------------------------------------------------------

; Compare the 4 Z-profiles obtained from the AOT1 experiments
```

```
; The routine called will correct HR6705 AOT1s for the known mispointing (1.3")
; as Z_corrected = Z + 1.3"
; A new normalisation to the nominal position is made via first
; interpolating the signals to a fine grid the Z_offsets (~0.2" step) and
; via the "spline_p" IDL routine, then re-normalising to the average
; signal around 0.5" of Z=0.

  set_plot,"ps"
  device,/landscape
  device,filename='ISOT04$DKB300:[DATA.AS.BEAMS]various_z_aot1s.ps'
  HR5340_1457_NML_6705_PLOT_ZPROFILES
  device,/close
  set_plot,"x"
```